Research Square

Preprints are preliminary reports that have not undergone peer review.
They should not be considered conclusive, used to inform clinical practice,
or referenced by the media as validated information.

A 2D-CFT Factory: Critical Lattice Models from Competing Anyon Condensation in SymTO

Ling Yan Hung

elektron.janethung@gmail.com

Tsinghua University https://orcid.org/0000-0002-0040-553X

Kaixin Ji

Fudan University

Ce Shen

Beijing Institute of Mathematical Sciences and Applications

Yu Zhao

Fudan University

Yidun Wan

Fudan University https://orcid.org/0000-0003-4318-8464

Article

Keywords:

Posted Date: September 17th, 2025

DOI: https://doi.org/10.21203/rs.3.rs-7547924/v1

License: This work is licensed under a Creative Commons Attribution 4.0 International License.
Read Full License

Additional Declarations: There is **NO** Competing Interest.

Version of Record: A version of this preprint was published at Nature Physics on September 14th, 2026.
See the published version at https://doi.org/10.1038/s41567-026-03438-6.

Prepared for submission to Nature

A 2D-CFT Factory: Critical Lattice Models from Competing Anyon Condensation in SymTO

Ling-Yan Hung[*a,c] **Kaixin Ji**[b] **Ce Shen**[c] **Yidun Wan**[*b,d,e] **Yu Zhao**[b]

[a] *Yau Mathematical Sciences Center, Tsinghua University, Beijing 100084, China*
[b] *State Key Laboratory of Surface Physics, Center for Astronomy and Astrophysics, Department of Physics, Center for Field Theory and Particle Physics, and Institute for Nanoelectronic devices and Quantum Computing, Fudan University, Shanghai 200433, China*
[c] *Beijing Institute of Mathematical Sciences and Applications, Beijing 101408, China*
[d] *Shanghai Research Center for Quantum Sciences, Shanghai 201315, China*
[e] *Hefei National Laboratory, Hefei 230088, China*

E-mail: lyhung@tsinghua.edu.cn, kxji21@m.fudan.edu.cn, scbebetterme@gmail.com, ydwan@fudan.edu.cn, yuzhao20@fudan.edu.cn

Abstract: In this paper, we introduce a "**CFT factory**" – a novel algorithm of methodically generating 2D lattice models that would flow to conformal field theories (CFTs) in the infrared. We realise these models by engineering the boundary conditions of 3D topological orders (SymTOs) described by string-net models. The critical points are induced by a commensurate condensation of non-commuting anyons. Our structured method generates an **infinite** family of critical lattice models, including the A-series minimal models, and uncovers previously unknown critical points. Notably, we discover at least three novel CFTs (with central charge $c \approx 1.3$, 1.8, and 2.5) that preserves the Haagerup symmetries, in addition to recovering previously reported examples. The non-invertible symmetries preserved at these points are dictated by a novel "refined condensation tree". The condensation trees, together with a generalised Kramers-Wannier (KW) duality, **predict** large swathes of phase boundaries and **sieves** out second order phase transitions. This predictive power is illustrated not only in well-studied examples, such as the 8-vertex model associated with the A_5 category, but also in new cases involving Haagerup symmetries, validated by an improved symmetry-preserving tensor-network renormalization group method. The critical couplings are precisely encoded in algebraic data (the Frobenius algebras and quantum dimensions of unitary fusion categories), thereby establishing a powerful and **systematic** route to the discovery and potential classification of new CFTs.

*Corresponding authors

Introduction

Critical lattice models are an exceedingly economical way of encoding conformal field theories (CFTs). Their systematic construction offers a promising avenue to classifying and solving for novel CFTs – a long-standing open problem, even in two dimensions where much more is understood. Ideally, a successful framework of critical lattice models should sufficiently constrain the models by physical principles (such as symmetries or matter content), such that the landscape can be explored in a controlled way. However, this goal faces two major challenges: First, engineering the desired physical properties of a lattice model is difficult; second, in the thermodynamic limit, generic lattice models tend to realize gapped phases, among which phase transitions are typically first order. To recover a CFT, a notorious challenge is to isolate second-order critical points.

Over the past five decades, significant efforts have been made to detect patterns in critical couplings. In some cases, criticality is observed in Kramers-Wannier (KW) self-dual models such as the Ising model. The notion of discrete holomorphicity [1–4] also provides a hint of the underlying patterns. About twenty years ago, a different line of progress emerged with the discovery of the so-called "golden chain" [5], a series of lattice models that were found to exhibit criticality protected by non-invertible symmetries. This model, along with a broad family of its generalizations [6–8] (often described by the "strange correlator" construction[1]), provides a concrete realization of the topological holographic principle [14–23]. In this framework, a transfer matrix with specified non-invertible symmetries can be expressed as the path integral of a higher-dimensional topological order (a symTO or symTFT), with appropriate boundary conditions. This so-called "sandwich construction" translates the search for CFTs with given (generalised) symmetries into the search for critical boundary conditions of the associated symTO. Although this problem remains open, recent progress has recast many integrable lattice models as strange correlators [6–8, 24, 25].

In this work, we propose a systematic solution to the decades-long challenge of constructing 2D critical systems. We establish a **CFT factory**: a systematic procedure for engineering boundary conditions in any given 2+1D string-net (SN) model [26], thereby generating infinite classes of 1+1D critical lattice models. By extending insights from models like the generalised golden chain, we connect the physics of competing anyon condensations to criticality. This allows us to control the minimal set of (often non-invertible) symmetries preserved in the construction, making it possible to systematically scan through the space of models and generate novel CFTs with specified symmetries.

The central mechanism of our factory, rooted in the topological holographic principle [5–8], is that the partition function of a 2D critical model can be realized as the overlap between a 2D gapped string-net wavefunction $|\Psi\rangle_{\mathrm{SN}(\mathscr{F})}$ and a specially designed boundary state $\langle\Omega_{\mathrm{critical}}|$:

$$Z_{2D\,\mathrm{critical}} = \langle\Omega_{\mathrm{critical}}|\Psi\rangle_{\mathrm{SN}(\mathscr{F})}. \tag{1}$$

[1] The strange correlator was first introduced in [9] to detect SPT phases, and later shown to be equivalent to studying non-trivial boundary conditions of 3D topological models. More recently, it has found diverse applications in constructing 1+1D phases, e.g. [10–13].

Here, $|\Psi\rangle_{\mathrm{SN}(\mathscr{F})}$ is a string-net model constructed from an input unitary fusion category (UFC) $\mathscr{F}$. The bulk topological phase described by this model has anyon types given by the simple objects of the Drinfeld center $\mathcal{Z}(\mathscr{F})$. We implement this model on a truncated square lattice (Fig. 1), where the vertex-plaquette equality in number plays an important role.

It was argued [27, 28] and proved rigorously [29] at least in the case of the 2D Ising model, that when a pair of non-commuting topological defects (which arises as anyons in the 3D symTO) remain unbroken (or uncondensed), the 2D model is either degenerate or gapless. In our construction, criticality emerges when this boundary state $\langle\Omega_{\mathrm{critical}}|$ enforces a commensurate balance of competing anyon condensates. The critical couplings and phase boundaries acquire a simple algebraic interpretation through the properties of the input $\mathscr{F}$. Specifically, the condensates are characterised by Frobenius algebras within $\mathscr{F}$. When competing anyons are commensurate in one unit cell, it turns out globally $\langle\Omega_{\mathrm{critical}}|\Psi\rangle_{\mathrm{SN}(\mathscr{F})}$ produces the partition function of a critical lattice model. By studying the competition of three competing condensates, we also produce analytical prediction of the location of phase boundaries. This is achieved by adjusting the amount of a third competing condensate in a way that does not disturb the equilibrium between the other two. The Hu–Geer–Wu (HGW) extension [30] of the Levin–Wen model proves to be a powerful tool to prepare condensates in a unit cell, as it resolves the internal spaces of anyons and allows for a finer analysis of their condensation [31, 32].

Meanwhile, we introduce a refined condensation tree to systematically track how the bulk symmetries are spontaneously broken, allowing us to predict the symmetries of the resulting CFT and engineer second-order phase transitions. Furthermore, many of the critical points we identify are shown to be self-dual under a generalised KW duality.

We demonstrate the power and validity of this framework with several key examples. As a first test, our approach naturally recovers an infinite family of well-known 2D models, including the A-series integrable models. In the 8-vertex models (duals of the Ashkin–Teller model) related to the A_5 string-net model, we analytically recover critical points previously known only through integrability and nearly determine the entire global phase diagram. We then showcase its predictive power by constructing novel lattice models with exotic Haagerup symmetries, including new critical theories not yet reported in the literature.

Across all tested examples, our analytical predictions show excellent agreement with highly accurate numerical results obtained using an improved symmetric Renormalization Group (sym-RG) method [8, 33, 34]. This combination of analytical theory and numerical verification provides a robust new pathway for exploring critical phenomena in 2D lattice systems.

Note that the form of $\langle\Omega|$ that recovers a RG fixed point, be it topological or conformal, is not unique. The universality of fixed points implies that many UV features in the lattice would be washed out under RG. Therefore, the seed state $\langle\Omega_{\mathrm{critical}}|$ that produces a CFT fixed point is not unique. The essence of our construction is to provide an algorithm to create a seed state that is destined to flow to a CFT in the infrared using only the category describing the symmetries of the CFT. This is thus a systematic *CFT factory*.

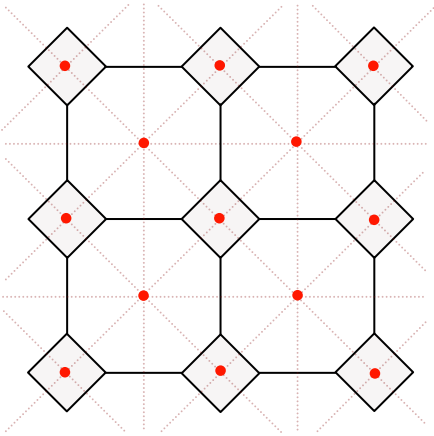


Fig. 1: The truncated square lattice and its dual triangulation $\{\Delta\}$.

Results

In our explicit construction of the strange correlator (1), the string-net model $|\Psi\rangle_{\mathrm{SN}(\mathscr{F})}$ is expressed as a projected entangled pair states (PEPS) in terms of quantum $6j$ symbols [7, 8]. This is reviewed in the supplementary materials, where $|\Psi\rangle_{\mathrm{SN}(\mathscr{F})}$ is broken down into a collection of triangles, and each triangle is given by the quantum 6j symbol of the input category $\mathscr{F}$. It can be interpreted as a 3D path-integral over a solid handle-body (say a solid ball), such that its boundary (say a sphere) is the 2D surface on which the lower dimensional theory is defined, as illustrated in Fig. 2. The state $\langle\Omega|$ can thus be understood as boundary conditions imposed on the 2D boundary of the 3D path-integral encapsulated in $|\Psi\rangle_{\mathrm{SN}(\mathscr{F})}$.

We want to construct a special state $\langle\Omega_{\mathrm{Critical}}|$ whose overlap with a string-net ground state $|\Psi\rangle_{\mathrm{SN}(\mathscr{F})}$, given input category $\mathscr{F}$, is a critical 2D partition function.

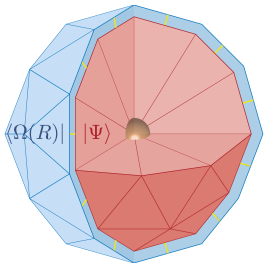


Fig. 2: Geometry of the strange correlator as a 3D path-integral. The Levin-Wen ground state $|\Psi\rangle_{\mathrm{SN}(\mathscr{F})}$ has a 3D TQFT realisation, which is chosen to be a sphere for concreteness. The state $\langle\Omega(R)|$ essentially determines the boundary condition of the 3D solid as a PEPS state. Its dependence on different couplings is denoted schematically by R. Their overlap produce a 2D partition function as in (1) on the surface of the ball. The inner hole (in brown) is up to a topological boundary condition for general sandwich construction, which in our current case is equivalent to filling up the hole.

In the square-octagon lattice shown in Fig. 1, the unit cell takes the shape of . We will be considering (almost) tensor product states. Namely, the global state $\langle\Omega|$ we consider can be constructed by specifying the state on the unit cell . First we construct a state in a unit cell with one type of anyon condensate characterised by a Frobenius algebra $\mathcal{A}$ in $\mathscr{F}$. Each $\mathcal{A}$ describes a *Lagrangian condensate* in the topological order $\mathcal{Z}(\mathscr{F})$ encoded in the $\mathscr{F}$-string-net model. A Lagrangian condensate L is a maximal condensate in $\mathcal{Z}(\mathscr{F})$ that breaks the topological phase to the trivial vacuum state.

A unitary Frobenius algebra $\mathcal{A}$ in $\mathscr{F}$ is a (possibly composite) object in $\mathscr{F}$:

$$\mathcal{A} = \bigoplus_{a\in\mathscr{F}} n_a a, \qquad n_a \in \mathbb{N}, \tag{2}$$

equipped with an algebra multiplication expressed as a cyclically symmetric function $f^{\mathcal{A}} : \mathcal{A}^3 \to \mathbb{C}$. That is, it is specified by a complex-valued tensor $f^{\mathcal{A}}_{abc*}$, for $a, b, c \in \mathcal{A}$. Here, $n_a \in \mathbb{N}$ is the multiplicity of simple object $a \in \mathscr{F}$ enrolled in $\mathcal{A}$. To avoid clutter, the discussion here is limited to $n_a \leq 1$, although it can be readily generalised. Similarly, a right module of a Frobenius algebra $\mathcal{A}$ in a UFC $\mathscr{F}$ is a (possibly composite) object

$$M_{\mathcal{A}} := \bigoplus_{x\in\mathscr{F}} m_x x,$$

equipped with an algebra action encoded by a *module function* $\rho_{M_{\mathcal{A}}} : \mathcal{A} \otimes {M_{\mathcal{A}}}^2 \to \mathbb{C}$. Similarly $\rho_{M_{\mathcal{A}}}$ is specified by a collection of complex numbers $[\rho_{M_{\mathcal{A}}}]^a_{bc}$ for $a \in \mathcal{A}$ and $b, c \in M_{\mathcal{A}}$. The properties of the algebra multiplication $f^{\mathcal{A}}$ and module function $\rho_{M_{\mathcal{A}}}$ are reviewed in the supplementary materials. It is crucial to point out that they can be solved algorithmically given $\mathscr{F}$. Now, explicitly a condensed state in one unit cell is given by

$$\langle\widehat{\mathcal{A}_i}|_{M_{\mathcal{A}_i}} := \frac{1}{N_{(\mathcal{A}_i,M_{\mathcal{A}_i})}} \langle \text{} | = \frac{1}{N_{(\mathcal{A}_i,M_{\mathcal{A}_i})}} \sum_{a\in\mathcal{A}} \sum_{x,y,u,v\in M_{\mathcal{A}}} \left\langle \text{} \right| [\rho_{M_{\mathcal{A}}}]^a_{xy} ([\rho_{M_{\mathcal{A}}}]^a_{uv})^*. \tag{3}$$

The four external slanted edges each carries a *right module* $M_{\mathcal{A}}$ of $\mathcal{A}$, and the horizontal/vertical edge between the slanted ones carries $\mathcal{A}$ itself. As shown in the supplementary material, this state is equivalent to a topological state describing the Lagrangian condensate characterised by $\mathcal{A}$ within one RG step as described in [33] for *any* choice of module $M_{\mathcal{A}}$ of $\mathcal{A}$. We propose that the normalisation $N_{(\mathcal{A}_i,M_{\mathcal{A}_i})}$ for the condensed state is given by

$$N^2_{(\mathcal{A},M_{\mathcal{A}})} \equiv \langle \text{} \rangle = d^2_{M_{\mathcal{A}}} d_{\mathcal{A}}, \tag{4}$$

where

$$d_{\mathcal{A}} = \sum_{a\in\mathcal{A}} n_a\, d_a, \qquad d_{M_{\mathcal{A}}} = \sum_{x\in M_{\mathcal{A}}} m_x\, d_x. \tag{5}$$

This normalisation – the most natural one in a fusion category $\mathscr{F}$ – follows from taking trace of the unit cell and its conjugate in the category $\mathscr{F}$, as depicted in Fig. 3.

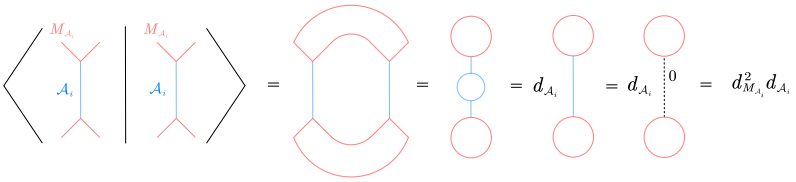


Fig. 3: Calculation of vertex normalization. In the second and third step we used the definition of module and algebra respectively. See the review in the supplementary materials for more detail.

A generic state involving the competition of multiple (normalised) Lagrangian condensates L_i, each characterised by a Frobenius algebra $\mathcal{A}_i$, is then given by the following linear combination:

$$\langle \{(r_i, \mathcal{A}_i, M_{\mathcal{A}_i})\}| = \sum_i r_i \langle \widehat{\mathcal{A}}_i|_{M_{\mathcal{A}_i}}, \tag{6}$$

where we require that

$$M_{\mathcal{A}_i} = M_{\mathcal{A}_j}$$

for all i, j appearing in the collection. This condition ensures that different unit cells do not interfere with each other, so we can tune individual unit cell to criticality and preserve the criticality globally. This is checked and discussed in further detail in the supplementary materials.

We propose that the location of the phase transition point between two competing anyon condensations L_i and L_j corresponding respectively to the Frobenius algebra $\mathcal{A}_i$ and $\mathcal{A}_i$ is given by the state.

$$\langle (\mathcal{A}_i, M_{\mathcal{A}_i}), (\mathcal{A}_j, M_{\mathcal{A}_j})|_{\text{critical}} = \langle \widehat{\mathcal{A}}_i|_{M_{\mathcal{A}_i}} + \langle \widehat{\mathcal{A}}_j|_{M_{\mathcal{A}_j}}. \tag{7}$$

Suppose the module M is shared by more than two phases. Then, there are phase boundaries between each pair of condensates. The phase boundary between a given pair of condensates characterised by $\mathcal{A}_i$ and $\mathcal{A}_j$ can be obtained by adding to the condensate the *perpendicular component to the vector connecting* $\mathcal{A}_i$ *and* $\mathcal{A}_j$ of another condensate $\mathcal{A}_k$. Specifically, we propose that a large part of the phase boundary between $\mathcal{A}_{i,j}$ (all the way up to a small vicinity of higher critical point between $\mathcal{A}_{i,j,k}$) can be traced out by state $\langle C_{ij}(p)|$ with a real parameter p as

$$\langle C_{ij}(p)| = \langle C_{ij}| + p \left(\langle \widehat{\mathcal{A}}_k| - \frac{\langle \widehat{\mathcal{A}}_k | B_{ij} \rangle}{\langle B_{ij} | B_{ij} \rangle} \langle B_{ij}| \right), \tag{8a}$$

where

$$\langle B_{ij}| = \langle \widehat{\mathcal{A}}_i| - \langle \widehat{\mathcal{A}}_j|, \tag{8b}$$

such that

$$\langle \widehat{\mathcal{A}}_i | C_{ij} \rangle_p = \langle \widehat{\mathcal{A}}_j | C_{ij} \rangle_p. \tag{8c}$$

The inner product is identical to the one used in (4). Physically, we are pouring into the cell $\mathcal{A}_k$ while preserving the balance between $\mathcal{A}_{i,j}$. For a generic phase diagram so obtained, we further derive the sufficient condition (eq. (17) in the Methods section) for all phase transitions therein to be second-order. These are the central results of the current paper. In the following, we will apply these results to different string-net models to generate explicit critical lattice models.

Critical States with Two Competing Condensates

For any given input category $\mathscr{F}$, consider a module M and the action ρ_M exactly shared by two algebras $\mathcal{A}_{i,j}$. The overlap between the string-net ground state with the boundary given by pairwise-competition (7) produces a critical lattice model. There are several classes of examples listed below and summarised in the tables 1-3 below.

1. Take $\mathscr{F} = A_{k+1}$ for $k \in \mathbb{Z}_{>0}$. For a given k it has $k+1$ simple objects $\{0, 1, \cdots, k\}$. For each $k \geq 2$, $1 \otimes 1 = 0 \oplus 2$. There are exactly two algebras, $\mathcal{A}_0 = 0$ and $\mathcal{A}_1 = 0 \oplus 2$ sharing the module consisting of the simple object 1. Their algebra multiplications and module functions are supplied in the supplementary material. Applying equation (7) reproduces the critical A-series integrable lattice models at second order phase transitions, which flows to the A-series minimal CFTs with central charge $c = 1 - \frac{6}{(k+1)(k+2)}$ in the thermodynamic limit [7, 33]. At $k = 2$, this reproduces the 2d classical Ising model at critical temperature $\beta = \beta_c = (\ln 1 + \sqrt{2})/2$ [6–8, 33].

2. Take $\mathscr{F} = \mathbb{Z}_p$ for all positive prime integers p. The simple objects are the $\mathbb{Z}_p$ group elements $\{0, \cdots, p-1\}$. Each $\mathbb{Z}_p$ has exactly two Frobenius algebras $\mathcal{A}_e = 0$ and $\mathcal{A}_m = \oplus_{i=0}^{p-1} i$, corresponding to pure electric condensate and pure magnetic condensate, in the $\mathcal{Z}(\mathbb{Z}_p)$ topological order described by the $\mathbb{Z}_p$ string-net model. They share the module $M = \mathcal{A}_m$, i.e., $\mathcal{A}_m$ is its own module and also $\mathcal{A}_e$'s module. Substituting into (7) produces the N-state Potts model at critical point, which is again the critical Ising model at $p = 2$, and for $p = 3$ this is the critical 3-state Potts model. Both of these are sitting at second order phase transitions. Note that for $p \geq 5$, these are critical points known to correspond to first order phase transitions. For $p = 5$, this is a weak first order transition related to a complex CFT [35, 36], whose central charge's real part can be detected by our sym-RG method. (See further discussion in the **Methods** section.)

3. Take $\mathscr{F} = H_3$, a category related to the Haagerup subfactor [37, 38]. The set of simple objects is $\{\mathbf{1}, \alpha, \alpha^2, \rho, \alpha\rho, \alpha^2\rho\}$. More details of the Haagerup category are supplied later and also in the supplementary material. Here, we note that for object ρ, $\rho \otimes \rho = \mathbf{1} \oplus \rho \oplus \alpha\rho + \alpha^2\rho$. This is a module shared precisely by two algebras $\mathcal{A}_0 = \mathbf{1}$ and $\mathcal{A}_1 = \mathbf{1} \oplus \rho \oplus \alpha\rho + \alpha^2\rho$. Substituting these to (7) is likely to produce the Haagerup anyon chain proposed in [25]. Our numerics however shows an approximate CFT with $c \approx 2.1$ that seems unstable to further RG, which needs extra future scrutiny.

4. One can consider other pairs of competing condensates in H_3. Between $\mathcal{A}_0$ above and $\mathcal{A}_2 = \mathbf{1} \oplus \alpha \oplus \alpha^2$, we can pick a common module given by $\mathcal{A}_2$ itself. In this

case, one can readily check numerically that the transfer matrix from (7) yields the 3-state Potts model, and this is the same model considered in [39]. There are three other mutually conjugated algebras $\mathcal{A}_{4,5,6}$ (details to be given later). The critical points between them and the $\mathcal{A}_0$ yields three similar CFTs. Their central charge are computed by our RG algorithms to be $c \approx 1.3$.

Critical States with More Competing Condensates and Phase Boundaries

We can also consider module M such that there are multiple algebras sharing the module, with the interpolation (6). For visual convenience, we mainly consider a sector with 3 competing algebras, i.e., moving in a phase space with two independent couplings up to an overall normalisation. Below are two classes of examples.

The A_5 strange correlator

The UFC A_5 has simple objects $\{0, 1, 2, 3, 4\}$. We shall focus on three Frobenius algebras (to be determined shortly) sharing the common module $M = 2$. Since

$$2 \otimes 2 = 0 \oplus 2 \oplus 4,$$

the unit cell is three-dimensional, with basis vectors $\langle$  | for $i \in \{0, 2, 4\}$. This choice corresponds to the 8-vertex model [7], or equivalently the Ashkin-Teller model [40–42].

There are four Frobenius algebras containing $\{0, 2, 4\}$. As evident in the refined condensation tree (Fig. 10), every Frobenius algebra includes elements from this set. At first sight, this might suggest that all such phases could appear under RG flows as we vary the relative weights of the basis states. But one can check that only three algebras sharing the same (right) module $M = 2$ actually emerge:

$$\mathcal{A}_0 = 0, \qquad \mathcal{A}_2 = 0 \oplus 4, \qquad \mathcal{A}_3 = 0 \oplus 2 \oplus 4. \tag{9}$$

Details of these algebras are given in the supplementary materials.

Again, the three pairwise competition points defined in (7) are all exactly second-order. Moreover, we plot the complete phase diagram in this two-dimensional parameter space with our symmetry-preserving RG method. It is shown in Fig. 4, adopting the parametrization

$$\langle (x, y, z)| \equiv x\langle$$  $$| + y\langle$$  $$| + z\langle$$  $$|. \tag{10}$$

The phase boundaries separating every pair of gapped phases are all second-order, and thus appear distinctly in the color plot of the central charge. In particular, two of the critical lines correspond to critical Ising CFT: one from the competition between $\mathcal{A}_{0,2}$, and the other from $\mathcal{A}_{2,3}$. These two lines intersect at the tri-critical point and merge into a self-dual $c = 1$ critical line associated with the competition between $\mathcal{A}_0$ and $\mathcal{A}_3$. We also observe that the two $c = 0.5$ Ising critical lines bend towards the $c = 1$ critical line near the tri-critical point – a feature that will reappear in other examples.

The thickness of the CFT lines, however, make it somewhat ambiguous where the precise location of the tri-critical point is. The A_5 model can be mapped to the isotropic

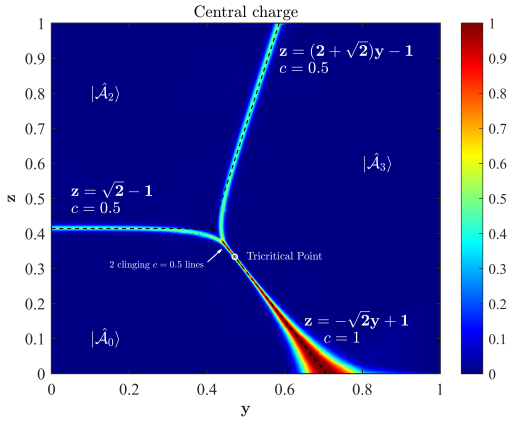


Fig. 4: Phase diagram of competing Frobenius algebras $\mathcal{A}_{0,2,3}$ with the slanted edge in the unit cell colored by the common module $M = 2$ in A_5, colored in numerically determined central charge corresponding to $\langle 1, y, z|$ as in (10). Each phase is marked by one of the nomalised states $\mathcal{A}_i$. The three phases are separated by critical lines with central charge $c > 0$. Dotted lines are the predicted critical states given in (11), derived from (8). A little above the tri-critical point, the two Ising lines are extremely close to each other (their distance is around $3 * 10^{-5}$ at $z = 0.35$), which merge into a fake $c = 1$ line. See the supplimentary materials for how we determine the tri-critical point.

Ashkin–Teller model, whose tri-critical point has been located via integrability. Translating back to the A_5 model, the tri-critical point is located at $\langle C_{03}|$, corresponding to the equilibrium state we constructed between $\mathcal{A}_0$ and $\mathcal{A}_3$. A magnified phase diagram obtained from the converged local tensor, together with the numerical determination of the tri-critical point, shows a much clearer match of the numerical tricritical point with $\langle C_{03}|$. These are presented in the supplementary materials. We now compare these phase boundaries to the predictions proposed in (8), which are obtained explicitly as

$$\begin{aligned} \langle C_{02}(y)| &= \langle 1, y, \sqrt{2} - 1|, \\ \langle C_{23}(y)| &= \langle 1, y, (2+\sqrt{2})y - 1|, \\ \langle C_{03}(y)| &= \langle 1, y, -\sqrt{2}y + 1|. \end{aligned} \tag{11}$$

These boundaries are shown as dotted lines in the plot. They agree well with the numerical phase boundaries everywhere except in a small region near the tri-critical point.

It is convenient to consider a triangular sub-region of Fig. 4 and map it to the vector space spanned by $\left(\langle\hat{\mathcal{A}}_2| - \langle\hat{\mathcal{A}}_0|\right)$ and $\left(\langle\hat{\mathcal{A}}_3| - \langle\hat{\mathcal{A}}_0|\right)$ as shown in Fig. 5. The three vertices correspond to the RG fixed-point condensate states $\langle\widehat{\mathcal{A}}_{0,2,3}|$. Notably, $|C_{02}\rangle_y$ and $|C_{03}\rangle_y$ are symmetric about $|C_{23}\rangle_y$, which is manifest in this ternary diagram. With the inner product defined as above, the pairwise competition points are located at the midpoints of the triangle's sides, and the predicted phase boundaries are given by its perpendicular bisectors. For the remainder of the paper, we will adopt this ternary phase diagram presentation, as it facilitates direct comparison with analytical predictions.

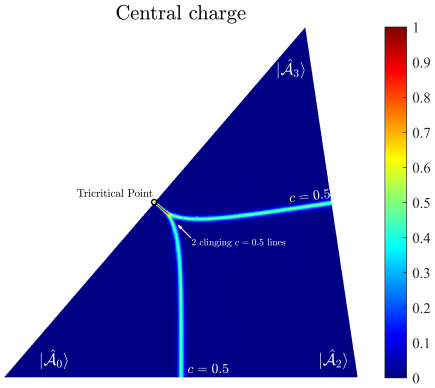


Fig. 5: Ternary phase diagram of Frobenius algebras $\mathcal{A}_{0,2,3}$ with module $M = 2$ in category A_5. Each vertex marks one of the three nomalised states as labelled in the figure, and any point within the triangle represents a weighted sum of these states. The three phases are seperated by the critical lines with central charge $c > 0$. These critical lines coincide well with the three perpendicular bisector of the triangle all the way up to a small region close to the tricritical point.

3-algebra competition in the Haagerup H_3 strange correlator - New CFT alert

The UFC H_3 has seven Frobenius algebras as follows:

$$\begin{aligned}
&\mathcal{A}_0 = \mathbf{1}, \quad \mathcal{A}_1 = \rho \otimes \mathcal{A}_0 \otimes \rho = \mathbf{1} \oplus \rho \oplus \alpha\rho \oplus \alpha^2\rho, \\
&\mathcal{A}_2 = \mathbf{1} \oplus \alpha \oplus \alpha^2, \quad \mathcal{A}_3 = \rho \otimes \mathcal{A}_2 \otimes \rho = (\mathbf{1} \oplus \rho \oplus \alpha\rho \oplus \alpha^2\rho) \otimes (\mathbf{1} \oplus \alpha \oplus \alpha^2), \\
&\mathcal{A}_4 = \mathbf{1} \oplus \rho \oplus \alpha\rho, \quad \mathcal{A}_5 = \alpha \otimes \mathcal{A}_4 \otimes \alpha^2 = \mathbf{1} \oplus \alpha\rho \oplus \alpha^2\rho, \\
&\mathcal{A}_6 = \alpha^2 \otimes \mathcal{A}_4 \otimes \alpha = \mathbf{1} \oplus \rho \oplus \alpha^2\rho.
\end{aligned}$$

Their modules and further details are in the supplementary materials.

According to these data, one can construct critical points from pairs of Frobenius algebras readily as in (7), some of which have been given above. Below are more non-exhaustive examples of competitions between these Frobenius algebras. Again, the location of all phase boundaries agrees amazingly well with the general prediction (8). The critical points are summarised in the tables 4 and 5 below. The central charges for new CFT candidates are numerical values, suggested by an $\approx$ sign. We also color them red for clarity.

1. **Competitions among $\mathcal{A}_{4,5,6}$ – New CFT alert** We first look at the three Frobenius algebras $\mathcal{A}_{4,5,6}$, related by conjugation by objects $\{\mathbf{1}, \alpha, \alpha^2\}$ that forms the $\mathbb{Z}_3 \in H_3$ subcategory. Each algebra $\mathcal{A}_{i=4,5,6}$ has a module $M_{\mathcal{A}_i}$ with the same object $\rho \oplus \alpha\rho \oplus \alpha^2\rho$ but equipped with different module functions. Their interpolations still take the form of (6) and plotted in the ternary Fig. 6, where this $\mathbb{Z}_3$ permutation symmetry is evident. Since the module functions for $M_{\mathcal{A}_{4,5,6}}$ are different, we have essentially turned on many different couplings and do not expect their pair competitions to generate second-order phase transitions. Indeed, the RG generates highly

fluctuating numerical central charge, which is also seen in our simulation of the Z_5 model that corresponds to a weak first-order phase transition. We are thus led to **conjecture that a fluctuating central charge is in fact a manifestation of the weak first order phase transitions in the proximity of a complex CFT**. Here, such fluctuations of the central charge in the vicinity of the critical point is even visible in the phase diagram. Along the phase boundaries, there are double line structures, with their centers of 0 central charge being the real phase transition lines. It is also pleasantly surprising that the **tri-critical point, which corresponds precisely to the equal weight summation of the three condensates, seems to be a novel CFT of** $c \approx 2.5$**.** A more accurate determination of the central charge of this CFT and its spectrum will be reported elsewhere.

2. **Competitions between** $\mathcal{A}_0$ **vs** $\mathcal{A}_{4,5,6}$ **– New CFT alert** As mentioned above, $\mathcal{A}_{4,5,6}$ are $\mathbb{Z}_3$ permutated. The pair competition between $\mathcal{A}_0$ and $\mathcal{A}_i$ for $i = 4, 5, 6$ produces the same critical point. For each i, as always possible because $\mathcal{A}_0 = \mathbf{1} \in \mathcal{A}_i$, we can pick the algebra $\mathcal{A}_i$ itself as the common module with $\mathcal{A}_0$. The common ancestor between $\mathcal{A}_0$ and any of the $\mathcal{A}_{4,5,6}$ goes all the way up to $\mathcal{Z}(H_3)$. We find that the pair-competition indeed produces a second-order phase transition that respects the full $\mathcal{Z}(H_3)$ symmetry. This is checked numerically, and **we found a novel critical point at** $c \approx 1.3$**, and potentially a new CFT in the IR.** Details of this model will be reported elsewhere.

3. We can also include any number of these six algebras $\mathcal{A}_{0,1,2,4,5,6}$ in the interpolation (6) , where we pick for each of them the common module $\rho + \alpha\rho + \alpha^2\rho$. We can keep any three phases in the interpolation and again plot ternary phase diagrams as in Fig. 7 and 8, still with vertices corresponding to the gapped RG fixed points. Because the phase diagram retains the permutation symmetry between $\mathcal{A}_{4,5,6}$, we will include them collectively in the diagram. The algebras $\mathcal{A}_{1,2}/\mathcal{A}_{4,5,6}$ do not share any module function, and they appear to produce indeed a first-order phase transition. The CFTs between other pair-competetions are already given above. **The tri-critical points provide various new critical points that potentially corresponds to new CFTs.** There are three tri-critical points with $c \approx 1.8$, one of which is plotted in Fig. 7. There are two tri-critical points with $c \approx 2.1$, one of which is plotted in Fig. 8. Results with better accuracy will be reported elsewhere.

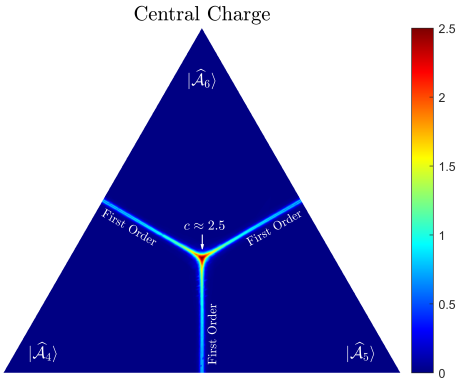


Fig. 6: The ternary phase diagram of interpolating Frobenius algebras $\mathcal{A}_{4,5,6}$ in the H_3 UFC. The slanted edges are colored by modules containing object $\rho \oplus \alpha\rho \oplus \alpha^2\rho$. Each phase is marked by one of the nomalised states $\mathcal{A}_i$. The tri-critical point is a CFT with $c \approx 2.5$. Equal weight summation of any pair of condensates does not produce a CFT. There are two traces of non-zero central charges for each of the first-order phase transitions. The actual phase transition lines sit at the center of these double lines. This may suggest a possible complex CFT at the vicinity of a weak first order as mentioned in the $\mathbb{Z}_5$ strange correlator. Improved accuracy and further simulations of the novel CFT will be reported elsewhere.

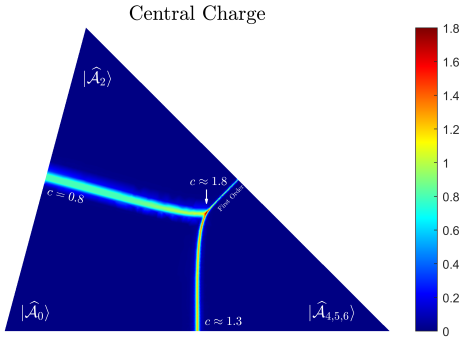


Fig. 7: The ternary phase diagram of interpolating Frobenius algebras $\mathcal{A}_{0,2,(4,5,6)}$ in the H_3 UFC. The slanted edges are colored by modules consisting of object $\rho \oplus \alpha\rho \oplus \alpha^2\rho$. Each phase is marked by a nomalised states $\mathcal{A}_i$. The three phases are seperated by the critical lines with central charge $c > 0$. CFT between $\mathcal{A}_0$ and $\mathcal{A}_2$ is the critical 3 state Potts model with $c = 0.8$. CFT between $\mathcal{A}_0$ and any of $\mathcal{A}_{4,5,6}$ has $c \approx 1.3$. Tri-critical point has $c \approx 1.8$. Phase transition point between $\mathcal{A}_2$ and any of the $\mathcal{A}_{4,5,6}$ is first-order. Appearance of non-zero central charges on the first order line are numerical fluctuations. Improved accuracy at the first order phase boundary and details of the novel CFTs will be reported elsewhere.

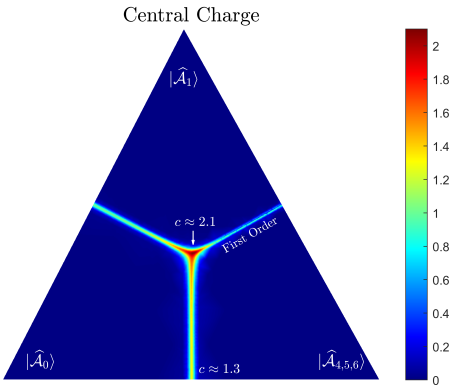


Fig. 8: The ternary phase diagram of interpolating Frobenius algebras $\mathcal{A}_{0,1,(4,5,6)}$ in the H_3 UFC. The slanted edges are colored by modules containing object $\rho \oplus \alpha\rho \oplus \alpha^2\rho$. Each phase is marked by one of the nomalised states $\mathcal{A}_i$. It is very close to a equilateral triangle but not. CFT between $\mathcal{A}_0$ and any of $\mathcal{A}_{4,5,6}$ has $c \approx 1.3$. The tri-critical point has $c \approx 2.1$. The phase transition between $\mathcal{A}_0$ and $\mathcal{A}_1$ is debatable; please see main text for details. Phase transition between $\mathcal{A}_1$ and any of the $\mathcal{A}_{4,5,6}$ is first-order. There are two traces of non-zero central charges. The vague one conincides with the actual phase transition line. The more clear one may suggest a possible complex CFT at the vicinity of the weak first order transition, similarly to the situation of the Z_5 strange correlator. Improved accuracy and further simulations of the novel CFT will be reported elsewhere.

Table 1: Critical points of pair competition in $Z_{2,3,4,5}$

Cat	Z_2	Z_3	Z_4			Z_5
$\mathcal{A}_i$	0	0	0		$0 \oplus 2$	0
$\mathcal{A}_j$	$0 \oplus 1$	$0 \oplus 1 \oplus 2$	$0 \oplus 2$	$0 \oplus 1 \oplus 2 \oplus 3$		$0 \oplus 1 \oplus 2 \oplus 3 \oplus 4$
M	$0 \oplus 1$	$0 \oplus 1 \oplus 2$	$0 \oplus 2$	$0 \oplus 1 \oplus 2 \oplus 3$		$0 \oplus 1 \oplus 2 \oplus 3 \oplus 4$
D_{unit}	2	3	2	4	4	5
Type	Second order					First order
CFT	Ising $c = 0.5$	3-Potts $c = 0.8$	Ising $c = 0.5$	4-Potts $c = 1$	Ising $c = 0.5$	–

Table 2: Critical points of pair competition in $A_{2,3,4}$

Cat	A_2	A_3	A_4					
$\mathcal{A}_i$	0	0	0			$0\oplus 2$		$0\oplus 3$
$\mathcal{A}_j$	$0\oplus 1$	$0\oplus 2$	$0\oplus 2$	$0\oplus 3$	$0\oplus 1\oplus 2\oplus 3$	$0\oplus 3$	$0\oplus 1\oplus 2\oplus 3$	
M	$0\oplus 1$	1	1	$0\oplus 3$	$1\oplus 2$			
D_{unit}	2	2	2	2	4	3	4	4
Type	Second order							
CFT	Ising $c=0.5$		tri-Ising $c=0.7$	Ising $c=0.5$	Ising $\otimes$ tri-Ising $c=1.2$		Ising $c=0.5$	tri-Ising $c=0.7$

Table 3: Critical points of pair competition in A_5

Cat	A_5						
$\mathcal{A}_i$	0			$0\oplus 4$		$0\oplus 2$	
$\mathcal{A}_j$	$0\oplus 2$	$0\oplus 4$	$0\oplus 2\oplus 4$	$0\oplus 2$	$0\oplus 2\oplus 4$		
M	1	2	2	$1\oplus 3$	2	$1\oplus 3^*$	$1\oplus 3^{**}$
D_{unit}	2	2	3	3	3	4	4
Type	Second order						First order
CFT	3-Potts $c=0.8$	Ising $c=0.5$	4-Potts $c=1$	Ising $\otimes$ 3-Potts $c=1.3$	Ising $c=0.5$	3-Potts $c=0.8$	–

* uses a connected module function while ** uses a disconnected one for the algebra $0\oplus 2$.

Table 4: Critical points of pair competition in H_3

Cat	H_3						
$\mathcal{A}_i$	$\mathcal{A}_0$			$\mathcal{A}_1$		$\mathcal{A}_2$	$\mathcal{A}_{4,5,6}$
$\mathcal{A}_j$	$\mathcal{A}_1$	$\mathcal{A}_2$	$\mathcal{A}_{4,5,6}$	$\mathcal{A}_2$	$\mathcal{A}_{4,5,6}$	$\mathcal{A}_{4,5,6}$	$\mathcal{A}_{(5,6),(4,6),(4,5)}$
M	$\rho\oplus\alpha\rho\oplus\alpha^2\rho$						
D_{unit}	4	3	3	6	6	5	5
Type	Second order			First order			
CFT	$c\approx 2.1$	3-Potts $c=0.8$	$c\approx 1.3$	–			

The central charges for new CFT candidates are numerical values, suggested by an $\approx$ sign and colored red.

Table 5: Tri-critical points of multipartite competitions in H_3

Cat	H_3							
$\mathcal{A}_i$	$\mathcal{A}_0$	$\mathcal{A}_0$	$\mathcal{A}_0$	$\mathcal{A}_1$	$\mathcal{A}_1$	$\mathcal{A}_0$	$\mathcal{A}_2$	$\mathcal{A}_4$
$\mathcal{A}_j$	$\mathcal{A}_1$	$\mathcal{A}_2$	$\mathcal{A}_1$	$\mathcal{A}_2$	$\mathcal{A}_{4,5,6}$			$\mathcal{A}_5$
$\mathcal{A}_k$	$\mathcal{A}_2$	$\mathcal{A}_{4,5,6}$	$\mathcal{A}_{4,5,6}$	$\mathcal{A}_{4,5,6}$	$\mathcal{A}_{(5,6),(4,6),(4,5)}$			$\mathcal{A}_6$
M	$\rho \oplus \alpha\rho \oplus \alpha^2\rho$							
D_{unit}	6	5	6	8	8	5	7	7
Type	Second order			First order		Second order		
CFT	$c \approx 1.8$	$c \approx 1.8$	$c \approx 2.1$	–	–	$c \approx 1.8$	$c \approx 2.1$	$c \approx 2.5$

The central charges for new CFT candidates are numerical values, suggested by an $\approx$ sign and colored red.

Discussion

In this paper, we have shown that non-commuting condensates could force the boundary of the 3D SymTO into criticality, thus generating 2D critical lattice models algorithmically. These models are well defined non-perturbatively, UV complete, and satisfy all the physical consistency conditions, such as modular invariance automatically. Our construction thus systematically generate novel CFTs that can be read off either by analytical analysis in the presence of integrability, or at least numerically. This could offer a powerful alternative route to the bootstrap program.

Our work lays key foundations for the Landau paradigm for lattice models. It is well known to be very difficult to write down an effective theory that incorporates given non-invertible symmetries that at the same time also carries detailed infrared dynamics of phase transitions. Such an effective theory description lies at the heart of the Landau paradigm because it allows a systematic method of constructing explicit and computable models, at least approximately. There, one focuses on the order parameters, which are generically limited to only a handful of fields and whose effective action can be written down systematically according to symmetries and scaling dimensions, that ultimately get reduced to a countable number of terms. To render the strange correlator equally powerful, we need to find the counterpart of order-paremeter field in the context of the strange correlator. **Our answer to this question is essentially the anyon creation operator in a unit cell.** (See also a companion paper [43] for explicit construction of order parameter fields.) Moving in phase space now corresponds simply to moving the vev of the order parameter in terms of the anyon condensate, thus providing physical handles in introducing different perturbations, and we can move in phase space in a physical and controlled manner. The mathematical framework of tensor category plays an essential role in making physical predictions here – suggesting that it is capturing crucial structures of phase transitions.

Methods

Condensation Tree and Determining the Amount of Symmetries Preserved

Anyon condensation is mathematically described by a twist-free, commutative, separable Frobenius algebra (CSFA) in the symTO characterised by the UMTC $\mathcal{Z}(\mathscr{F})$. One twist-free CSFA[2] $\mathbf{A}_1$ can be a sub-algebra of a bigger one $\mathbf{A}_2$, i.e., $\mathbf{A}_1 \subset \mathbf{A}_2$. When this occurs, $\mathbf{A}_2$ can be condensed in two steps: first condensing anyons in $\mathbf{A}_1$, then condensing some other unconfined anyons over the $\mathbf{A}_1$ condensate to obtain the aggregate $\mathbf{A}_2$ condensate. Therefore, the sub-algebra $\mathbf{A}_1$ can be considered as a parent of $\mathbf{A}_2$. Such considerations produce a hierarchy of condensates [14, 20, 44] that can be conveniently arranged as a tree, which was dubbed a Hasse diagram [44], where each node corresponds to a condensable algebra, and an edge connects one node to a subalgebra node. Lagrangian algebras are those twist-free CSFAs corresponding to maximal condensates – such that the resultant phase is topologically trivial – that would appear as bottom nodes of the tree. That is,

[2] We use a bold letter $\mathbf{A}$ for a CSFA in the output data $\mathcal{Z}(\mathscr{F})$ of the HGW model, compaired with the curly letter $\mathcal{A}$ for a Frobenius algebra in an input UFC $\mathscr{F}$.

we start from the trivial twist-free CSFA including only the identity object, which is a sub-algebra to all other algebras, as the top node of the tree and grow the tree downwards.

The key refinement of our condensation tree over Hasse diagrams previousely considered [44] is the inclusion of Morita equivalent Frobenius algebras in the input category $\mathscr{F}$ as physically distinguishable condensates. While these algebras correspond to the same set of condensed anyons in the output theory, they produce physically distinguishable gapped phases [32, 33, 43], such that non-trivial phase transitions between them can in fact occur, as is evident in the previous discussion. They correspond to distinct symmetry breaking patterns that arise from non-trivial internal degrees of freedom of the condensing anyons[31, 32, 43], and such details are made explicit in the HGW model. Meanwhile, we note that intermediate phases where some non-maximal set of anyons condensed in the output theory can be described by sub-category[3] $\mathcal{K}$ of the input category $\mathscr{F}$[32]. This is natural since a non-trivial condensate would take the bulk symTO to a child topological order, and the corresponding degrees of freedom on the lattice is expected to be reduced to some subset of $\mathscr{F}$. When the condensate L_i in the symTO is Lagrangian, the corresponding HGW string-net model is projected effectively down to one-dimensional, reflecting the fact that the corresponding condensed phase is topologically trivial. In the condensed phase, each edge is projected to the chosen Frobenius algebra $\mathcal{A}_i$ corresponding to L_i. For instance, if we select the trivial Frobenius algebra $\mathcal{A}_0 = \mathbf{1}$, the resulting child model has only a single physical state, where every edge is labeled by the trivial degree of freedom 1. We are now ready to introduce the refined condensation tree as follows. Each node is labeled by a subcategory $\mathcal{K}$ of $\mathscr{F}$. Note that the identity object of a subcategory $\mathcal{K}$ is, in general, a composite object in $\mathscr{F}$ unless $\mathcal{K}$ is a full subcategory. The requirement that $\mathcal{K}$ possesses an identity object is precisely the requirement that there exists a separable Frobenius algebra – after all, the defining property of a separable Frobenius algebra is that the composite object $\mathcal{A}$ is strictly associative under fusion, and that "bubbles" (trivial summands) can be freely included or removed. Thus, the identity object of $\mathcal{K}$ is given by a Frobenius algebra $\mathcal{A}$, and the remaining objects in $\mathcal{K}$ are precisely the bimodules over $\mathcal{A}$.

Two nodes are connected by an edge if the identity object of $\mathcal{K}_i$, given by a Frobenius algebra $\mathcal{A}_i$, is a subalgebra of the identity object $\mathcal{A}_j$ of $\mathcal{K}_j$, and $\mathcal{A}_j$ can be obtained from $\mathcal{A}_i$ as a Frobenius algebra in the subcategory $\mathcal{K}_i$.

The above statements are essentially rephrasing the relation between two nodes in the original Hasse diagram – namely that a node is connected to another if the latter phase can be obtained from the former by anyon condensation. The refined condensation tree contains more nodes in general.

Here are a few examples. The simplest example is the symTO corresponding to the doubled Ising model. Recall that there are three objects denoted $\mathbf{1}, \sigma, \psi$ in the input Ising UFC, and there are two connected Frobenius algebras $\mathcal{A}_0 = \mathbf{1}$ and $\mathcal{A}_1 = \mathbf{1} \oplus \psi$. The corresponding refined condensation tree is shown in Fig. 9.

A more interesting example is the condensation tree for $k = 4$. In the refined conden-

[3] A simple object of $\mathcal{K}$ may be a nonsimple object of $\mathscr{F}$.

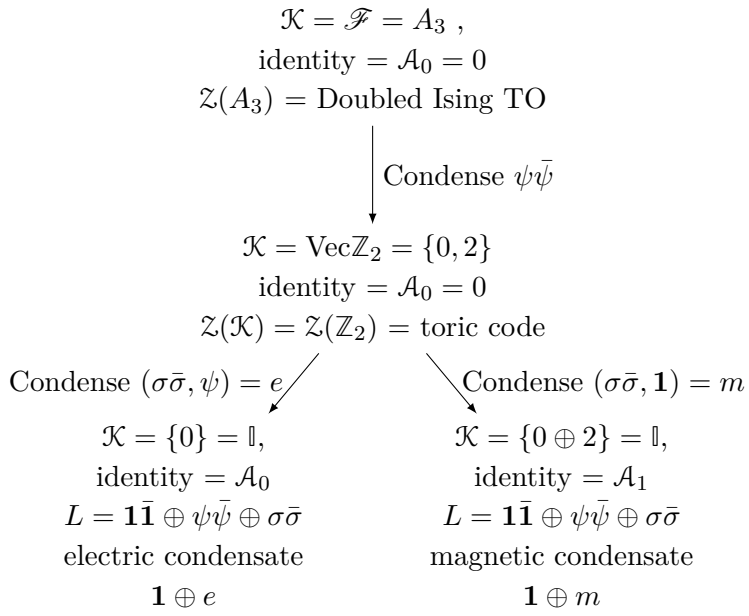


Fig. 9: Condensation tree for the doubled Ising TO. Each link is graced with the output bulk anyons that condensed. Each node is a subcategory and also the corresponding output condensed phase.

sation tree for the symTO $\mathcal{Z}(A_5)$,

$$L_0 = \oplus_{i=0}^{4} i\bar{i}, \qquad L_1 = (0 \oplus 4)\overline{(0 \oplus 4)} \oplus 2\ 2\bar{2}. \tag{12}$$

At the bottom of Fig. 10, we express each Lagrangian algebra also as comprised of anyons in the intermediate condensed phase $\mathcal{Z}(S_3)$. The latter has 8 different anyons, and they are related to the anyons of $\mathcal{Z}(A_5)$ as shown in the following table.

It is evident from a refined condensation tree that there is a notion of distance between Frobenius algebras. Down the tree, nodes denote symTO with more symmetries spontaneously broken by anyon condensation. The minimal amount of symmetry preserved in the critical state obtained from the competing pair of Frobenius algebras—assuming that we managed to choose appropriate modules M to sieve out first order phase transitions – **is determined by the first common ancestor node of the pair.** The topological excitations carried by the symTO of the ancestor node are the minimal set of symmetries that are preserved by the gapless phase. The resulting CFT may exhibit emergent symmetries beyond those of the ancestor node but cannot have fewer.

Let us revisit the examples we have considered to illustrate these ideas.

1. **Critical theory from the doubled Ising symTO** In the case of the Ising spin model (or the A_3 model), the first common ancestor of $\mathcal{A}_0$ and $\mathcal{A}_2$ is the node corresponding to $\mathcal{Z}(\mathbb{Z}_2)$, as shown in Fig. 9. Therefore the minimal set of topological symmetries is characterised by the toric code order, which has 3 non-trivial topological excitations corresponding to a $\mathbb{Z}_2$ electric charge, a magnetic flux, and their

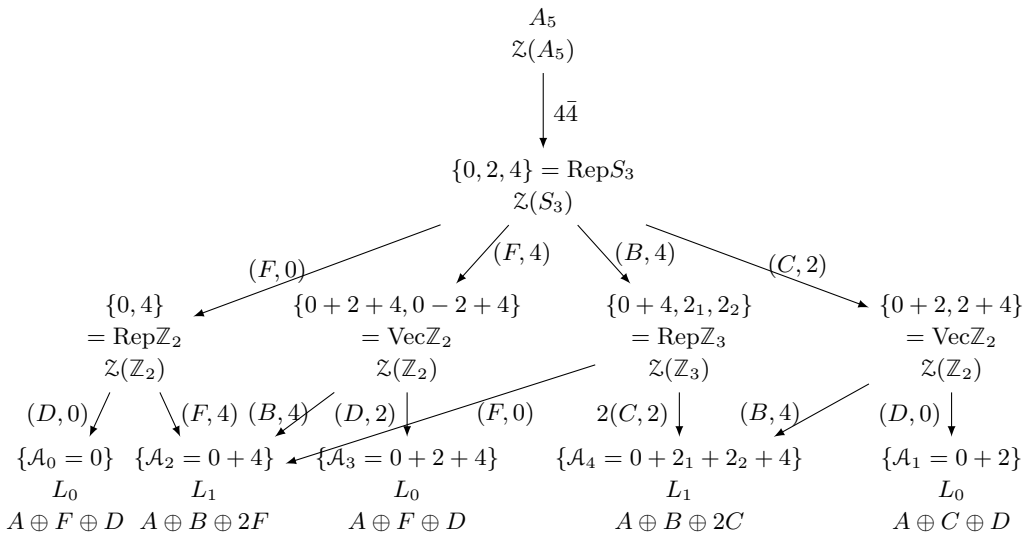


Fig. 10: The condensation tree for the Doubled A_5 symTO. In the second layer of arrows we indicate the intermediate condensing anyons using anyon labels in $\mathcal{Z}(S_3)$ to avoid clutter. In the last layer, we also include the condensate as anyons in the $\mathcal{Z}(S_3)$ phase. As we move down the tree, simple anyons in the partially condensed symTO corresponding to the lower nodes are composites in the parent nodes. Hence, the condensing anyons expressed in terms of $\mathcal{Z}(S_3)$ anyon that label the bottom layer of arrows are only representatives of a group of anyons in $\mathcal{Z}(S_3)$ that are identified in the child $\mathbb{Z}_2$ and $\mathbb{Z}_3$ nodes. The second index in the bracket indicates the microscopic degrees of freedom that take part in the condensation. The meanings of these symbols are explained in the previous section.

bound state. The actual symmetry of the Ising CFT is enlarged to the full Ising category, describable by the top node.

2. **Critical theories from the A_5 symTO**

   (a) The first common ancestor of $\mathcal{A}_0$ and $\mathcal{A}_2$ is $Z(\mathbb{Z}_2)$. Their competition is identical to the case of the Ising spin model and we expect the critical point to be the Ising CFT. Similarly, the competition of $\mathcal{A}_2$ and $\mathcal{A}_3$ is also expected to be Ising.

   (b) The first common ancestor of $\mathcal{A}_2$ and $\mathcal{A}_3$ is $\mathcal{Z}(\mathbb{Z}_3)$. As we discussed above, the electric/magnetic competition in $\mathcal{Z}(\mathbb{Z}_3)$ in a unit cell produces the 3-state Potts model. This is indeed inherited in the competition between $\mathcal{A}_2$ and $\mathcal{A}_3$.

   (c) The competition between $\mathcal{A}_0$ and $\mathcal{A}_3$ should produce a CFT that sees at least symmetries in $\mathcal{Z}(S_3)$, which is their common ancestor. This is indeed confirmed. The critical point constructed by their equilibirum point is given by a free boson CFT with $c = 1$.

   (d) The competition between $\mathcal{A}_0$ and $\mathcal{A}_4$ should also produce a CFT that preserves at least the symmetry imposed by $\mathcal{Z}(S_3)$. In fact, this CFT is the minimal model in the A series at $k = 4$, with $c = 4/5$. Its complete set of topological symmetries are in fact characterised by $\mathcal{Z}(A_5)$.

$\mathcal{Z}(\mathtt{Rep}S_3)$ Anyon Type	$\mathcal{Z}(\mathtt{Rep}S_3)$ Dyon Type	$Z(A_5)$ Dyon Types
A	$(A,0)$	$(0\bar{0},0),(4\bar{4},0)$
B	$(B,4)$	$(0\bar{4},4),(4\bar{0},4)$
C	$(C,2)$	$(2\bar{2},2)$
D	$(D,0)$	$(1\bar{1},0),(3\bar{3},0)$
	$(D,2)$	$(1\bar{1},2),(3\bar{3},2)$
E	$(E,2)$	$(1\bar{3},2),(3\bar{1},2)$
	$(E,4)$	$(1\bar{3},4),(3\bar{1},4)$
F	$(F,0)$	$(2\bar{2},0)$
	$(F,4)$	$(2\bar{2},4)$
G	$(G,4)$	$(0\bar{2},2),(4\bar{2},2)$
H	$(H,4)$	$(2\bar{0},2),(2\bar{4},2)$

Table 6: Relation between $\mathcal{Z}(\mathtt{Rep}S_3)$ anyons and $\mathcal{Z}(A_5)$ anyons.

These examples completely confirm our expectations by means of our refined condensation trees.

Cutting Down Phase Space to Avoid First Order Phase Transitions

As aforementioned, when competing anyons are at a tie, it is expected that the resultant phase is either gapless or degenerate. The latter corresponds to first order phase transitions from the perspective of the 2D classical statistical lattice model. Usually at a first order phase transition between two phases, the free energies of the respective phases become equal, and that is the classical interpretation of degeneracies in the 1+1 D quantum model.

In our construction of the lattice model, we focus on a unit cell with 5 edges. The dimension of phase space is thus reduced to roughly speaking $|\mathscr{F}|^5$, where $|\mathscr{F}|$ denotes the number of simple objects of $\mathscr{F}$. A generic state $\langle\Omega|$ on our unit cell is far from any RG fixed point. The interpolation (6) at first sight involves a small number of couplings compared with $|\mathscr{F}|^5$. Under RG, however, all other linear combination of the fusion channels in the unit cell could be invoked, i.e., the dimension of possible couplings is much greater than the number of gapped phases nearby described by Frobenius algebras. In such cases, there would be plenty of room for first order phase transitions.

In principle, as in the golden chain and other cases considered in [5–8], the strange correlator construction imposes (non-invertible) topological symmetries in the 2D theory.

Nonetheless, it is generally unclear how to ensure that the symmetry is not broken spontaneously in the quantum spin-chain by $\langle\Omega|$.

To exclude first-order phase transitions or degeneracies, the key is to reduce the dimension of phase space as much as possible: We need to reduce the number of new fusion channels that are generated under RG in much of the space of couplings. Choosing a coupling sourcing a specific gapped phase described by a Frobenius algebra in the unit cell, it would quickly converge to the gapped fixed point state (3) under RG, i.e., a coupling turned on for a given Frobenius algebra is essentially located within *the basin of attraction* under RG to a fixed point. In such a case, new fusion channels are not generated. In other words, it is desirable to choose (6), such that we are restricted to fewer attraction basins for the space of couplings we explore.

One could count the dimension of couplings introduced as follows. The coefficient of each state $\sum_{x,y,u,v\in M}$  $[\rho_{M_\mathcal{A}}]^a_{xy}([\rho_{M_\mathcal{A}}]^a_{uv})^*$ for a fixed a where $a \in \mathcal{A}_i$ constitutes an independent coupling in this reduced phase space. $N_\mathcal{A}$ is the number of objects in $\mathcal{A}$. Recall that to decouple different unit cells, we required that all $M_{\mathcal{A}_i}$ considered in a competition of condensates share the same set of module objects. As such, we can simply denote this common module by M; however, for the most generic case, the algebra actions of $\mathcal{A}_i$ and $\mathcal{A}_j$ on M may differ. In such a case, any basis element in each Frobenius algebra $\mathcal{A}_i$ introduces an independent linear combination of the fusion channel $\sum_{x,y,u,v\in M}$  $[\rho_{M_\mathcal{A}}]^a_{xy}([\rho_{M_\mathcal{A}}]^a_{uv})^*$. For a certain basis element $a \in \mathcal{A}_i \cap \mathcal{A}_j$, when it acts identically as an element of $\mathcal{A}_i$ and as an element of $\mathcal{A}_j$ on M, a single linear combination of fusion channel is attached to this element a. We refer to such a shared basis element a a *perfectly shared element*, and if the common elements of all algebras are perfectly shared on M, we term M a *perfect common module* for these algebras. Therefore, we can count the dimension D_{unit} of vector space in a unit cell as follows:

$$D_{\text{unit}} = \sum_i N_{\mathcal{A}_i} - \sum_{\text{perfectly shared } a} (N_a^{\text{common}} - 1), \tag{13}$$

where N_a^{common} is the number of algebras $\mathcal{A}_i$ having a perfectly shared element a. For example, if a is perfectly shared by two algebras acting on M, $N_a^{\text{common}} = 2$. In particular, the identity object on any M is always a perfectly shared element of all Frobenius algebras of a UFC. So for n algebras sharing a module, $N_{\text{identity}}^{\text{common}} = n$. Since the overall normalisation of the state $\langle\Omega|$ is physically irrelevant in the strange correlator, $D_{\text{unit}} - 1$ gives the dimension D_{c} of phase space – the number of independent couplings – introduced in the ansatz, i.e.,

$$D_{\text{c}} = D_{\text{unit}} - 1. \tag{14}$$

For two competing algebras only, the number of degrees of freedom introduced in a unit cell is reduced to

$$D_{\text{unit}}(\mathcal{A}_i, \mathcal{A}_j) = N_{\mathcal{A}_i} + N_{\mathcal{A}_j} - N_{\text{perfectly shared } a}, \tag{15}$$

where $N_{\text{perfectly shared } a}$ directly counts the number of perfectly shared element $a \in \mathcal{A}_i \cap \mathcal{A}_j$.

There is a special case in which the D_{unit} is reduced most drastically, That is to choose a perfect common module M of all competing Frobenius algebras $\mathcal{A}_i$. This can be typically achieved when the competing algebras are ordered as sub-algebras of one another: $\cdots \subset \mathcal{A}_i \subset \mathcal{A}_j \subset \mathcal{A}_k$. Suppose $\mathcal{A}_i \subset \mathcal{A}_j$, they must share a common ancestor in the refined condensation tree, where the identity object of the sub-input-category $\mathcal{K} \subset \mathscr{F}$ is given by the smaller Frobenius algebra $\mathcal{A}_i$. In the said special case,

$$D_{\text{unit}}(\cdots \subset \mathcal{A}_i \subset \mathcal{A}_j \subset \mathcal{A}_k) = N_{\mathcal{A}_k}. \tag{16}$$

That is, the number of degrees of freedom is simply given by the number of objects in the largest algebra among all algebras sharing the same perfect common module M.

One can show that the choice of perfect common module M is immaterial: Within one step of symmetric RG (as discussed in the Methods section), $\langle\Omega(M)|$ constructed from interpolations of normalised Frobenius algebras with module M in each unit cell reduces to the same state $\langle\Omega|$ for all choices of M, up to overall normalisations depending on the quantum dimension of M.

Now for a choice of perfect common module M shared only by n_M different Frobenius algebra among all competing ones, we note that all other gapped phases corresponding to Frobenius algebras not sharing M would not occur under RG. The RG attraction basins would be restricted to those gapped phases that share this M. This is an effective method to reduce the possibilities of gapped phases showing up in the reduced phase space.

If $D_c = D_{\text{unit}} - 1$ is larger than the number n_M of algebras $\mathcal{A}_i$ sharing the module M ($1 \leq i \leq n_M$, and n_M is the number of gapped phases allowed in the reduced phase space), there is naviely still room for degeneracies and thus room for first order phase transitions. We thus arrive at the following *sufficient condition* for second order phase transitions:

All phase transitions in a phase diagram are forced to be second order if

$$n_M > D_c. \tag{17}$$

When (17) is satisfied, the number of competing anyon condensates is greater than the number of independent degrees of freedom within a unit cell that can be varied. Therefore consider tuning a pair of condensates to be commensurate, changing the weight of any of the $D_c - 1$ independent coefficients correspond to moving in a direction towards another condensate that cannot be condensed at the same time as the pair anyway, leaving no room for degeneracy.

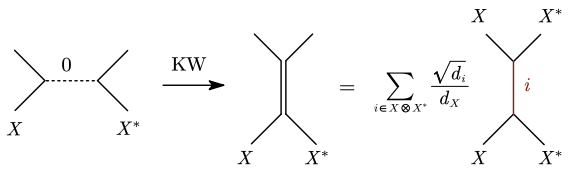
One can check this condition for the A-series minimal models for all k discussed above. There, $D_c = 1$ and $n_M = 2$, and the critical points are all second order, and flow to the A-series minimal models in the thermodynamic limit. The N-state Potts models can be constructed from the $\mathbb{Z}_N$ string-net model. The critical point is located at the transition point exactly as predicted in (7), from a competition between the Frobenius algebra $\mathcal{A}_e = 0$ corresponding to all electric condensate, and $\mathcal{A}_m = 0 \oplus 1 \oplus \cdots \oplus N-1$ corresponding to all magnetic condensate. In this case, $D_c = N$ and $n_M = 2$ wherever N is prime. It is well known that for $N \geq 5$, the critical point is first order, consistent with the counting here. One can also check with the critical models following from the Haagerup string net

model discussed above, and find that indeed they are consistent with the rule here. Note that our condition for second-order phase transition is only sufficient, not necessary, so it is overly strong and could potentially leave out many CFTs. For example in the case for $\mathbb{Z}_N$ where $N = 3$, i.e., the 3-state Potts model, by our counting, the commensurate state of $\mathbb{Z}_3$ could potentially give a first-order phase transition, but it is in fact a well-known second order transition. This also happens in the Haagerup models, in which novel continuous transitions are confirmed numerically even though we have not cut down the phase space sufficiently. We believe that our condition can be relaxed in the future.

Generalised Kramers-Wannier Duality

The Kramers-Wannier duality is a duality transformation in statistical mechanics that relates the ordered and disordered phases of a system. The phase transition point between these two phases coincide with the self-dual point, where the system often exhibits critical behavior. For example, in the classical Ising model, the KW duality relates the high- and low-temperature phases. The critical temperature is found to coincide with the self-dual point. In $\mathbb{Z}_N$ lattice models, KW duality refers to a Fourier-type transform of couplings [45–47]. In these cases, the KW duality is essentially the electromagnetic duality, which exchanges the electric and magnetic charges of the global $\mathbb{Z}_N$ symmetry of the lattice model. ($N = 2$ for the Ising model.)

In our construction, it turns out that these KW dualities known in the literature can be understood as a transformation that maps the original strange correlator on the square-octagon lattice to a strange correlator on the dual lattice. An advantage of using the square-octagon lattice is that its dual lattice has the same shape: The dual lattice exchanges the squares and octagons of the original lattice. This exchange is achieved by making an F-move on every octagon edge, as shown in Fig. 11 with the example of A_{k+1} series. The F-move used here is applicable to any trivial Morita class: for any $\mathcal{A} = X \otimes X^*$ with $M = X$, we have



(18)

There is thus a self-dual point in the interpolation between $\mathcal{A} = 0$ and $\mathcal{A} = X \otimes X$ that is invariant under KW. In the case of the A-series CFTs, the self-dual point is $\langle$  $| + \frac{d_1-1}{\sqrt{d_2}} \langle$  $|$, which exactly matches the critical points obtained by the equal sum of normalized states.

We can also apply (18) to analyze the competition between $\mathcal{A}_0 = \mathbf{1}$ and $\mathcal{A}_1 = \rho \otimes \rho$ in the H_3 with ρ as a perfect common module. The duality transformation maps ρ-squares to ρ-octagons, and the double ρ-lines on an octagon edge is equivalent to $\sum_{i\in\rho\otimes\rho} \frac{\sqrt{d_i}}{d} i$ lines. Then we can verify that the system is self-dual when the octagon edge takes the state

$$|1\rangle + \frac{1}{\sqrt{3d+1}} \left(|1\rangle + \sqrt{d}|\rho\rangle + \sqrt{d}|\alpha\rho\rangle + \sqrt{d}\left|\alpha^2\rho\right\rangle \right)$$

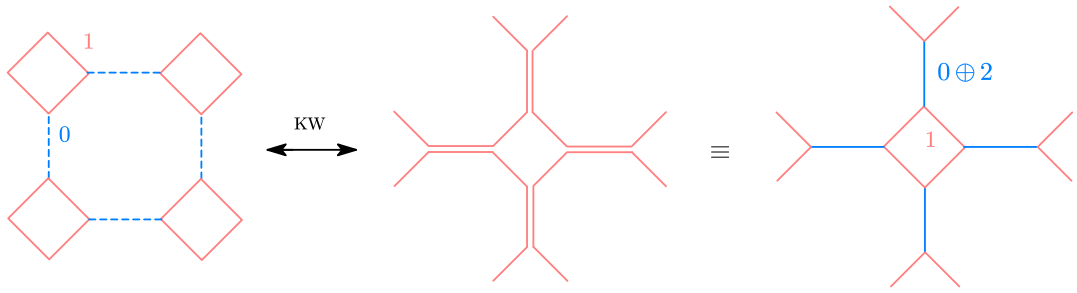


Fig. 11: Generalised KW duality for the A_{k+1} category. The common module is 1 and the competing Frobenius algebras are $\mathcal{A}_1 = 0$ and $\mathcal{A}_2 = 0 \oplus 2$. Under KW duality the 1-squares are mapped to 1-octagons, and the positions of squares and octagons are exchanged. The horizontal and vertical octagon edges are exchanged under KW. The double 1-line on the octagon edge is equivalent to algebra $\mathcal{A}_2$ ending on the module $M = 1$. So we see that the two gapped phases given by $\mathcal{A}_1$ and $\mathcal{A}_2$ are KW dual to each other. The self-dual point is obtained by requiring that the unit cell is invariant under an F-move, which exactly matches critical point obtained by the equal sum of normalised states.

This self-dual point again coincides precisely with the point calculated by (7).

This duality can even be applied to compute tri-critical points, via a double-layer construction. We consider interpolating among $\mathcal{A}_{0,2,3}$ in A_5 with $M = 2$ as an example. The unitcell is three dimensional with basis $|\, i \,\rangle$, $i \in \{0, 2, 4\}$. The KW duality is performed by doing an F-move on every octagon edge. This operation is represented by:

$$|\, 0 \,\rangle \xrightarrow{F} \frac{1}{2}\left(|\, 0 \,\rangle + \sqrt{2}|\, 2 \,\rangle + |\, 4 \,\rangle\right),$$
$$|\, 2 \,\rangle \xrightarrow{F} \frac{1}{\sqrt{2}}\left(|\, 0 \,\rangle - |\, 4 \,\rangle\right),$$
$$|\, 4 \,\rangle \xrightarrow{F} \frac{1}{2}\left(|\, 0 \,\rangle - \sqrt{2}|\, 2 \,\rangle + |\, 4 \,\rangle\right).$$

As explained in Fig. 11, F-moves map the vertical edges to horizontal edges. After doing F-moves, we have implicitly shifted the lattice by a unit cell, shifting our focus on the vertical edges shown on the right-hand side.

In what follows, we denote the basis $|\, i \,\rangle$ by $|i\rangle$. Under the normalization where $|0\rangle$ has a coefficient of 1, the parameter space is two-dimensional, with a generic point represented as $|0\rangle + y|2\rangle + z|4\rangle$. The KW duality acts as a transformation on this parameter space, mapping it onto itself. The KW self-dual points correspond to the fixed points of this transformation. In this case, the self-dual points lie along a line in the parameter space, given by the equation:

$$z = -\sqrt{2}y + 1. \tag{19}$$

The phase boundary between $\mathcal{A}_0$ and $\mathcal{A}_2$ completely lie on the KW self-dual line and ends at the tricritical point as in Fig. 4. The $\mathcal{A}_0$ phase is centered at the point

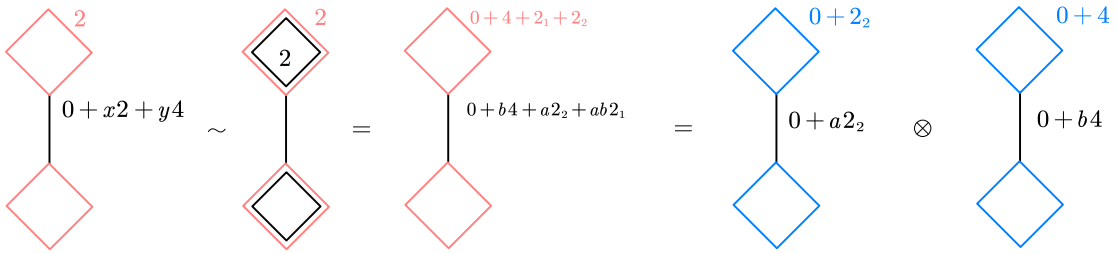


Fig. 12: Double layer of Ising models.

($y = 0, z = 0$), and the $\mathcal{A}_2$ phase is centered at the point ($y = \sqrt{2}, z = 1$). The interpolating line connecting the two points intersects the KW self-dual line at the point ($y = \frac{\sqrt{2}}{3}, z = \frac{1}{3}$), which is exactly the critical point constructed by the equilibrium state of $\mathcal{A}_0$ and $\mathcal{A}_2$.

Next, we show how the A_5 model is related to two copies Ising models and derive the critical points and the tricritical point in the phase diagram. The simple object 2 in A_5 is the two dimensional irrep of Rep(S_3). This fact motivates us to split the simple object 2 into two quasi-objects 2_1 and 2_2 with quantum dimensions equal to 1[31, 32, 43]. We make two assumptions about the quasiobjects and show that under these assumptions we can decompose the system into two Ising models and calculate precisely the critical points and the tricritical point.

Assumption 1: as quasiobjects

$$2 = 2_1 \oplus 2_2, \qquad 2_2 \otimes 2_2 = 0, \qquad 4 \otimes 2_1 = 2_2, \qquad 4 \otimes 2_2 = 2_1$$

Assumption 2: as states in local Hilbert space

$$\frac{1}{\sqrt{2}}\left(|2_1\rangle + |2_2\rangle\right) = |2\rangle, \qquad \frac{1}{\sqrt{2}}\left(|2_1\rangle - |2_2\rangle\right) = \frac{1}{\sqrt{2}}\left(|0\rangle + |4\rangle\right).$$

For the current strange correlator the module is 2, and up to a global constant we can add a loop labeled by 2 in all the squares, this turns the module to $2 \otimes 2$. Under our assumption, the module is now $2 \otimes 2 = 0 \oplus 2_1 \oplus 2_2 \oplus 4 = (0 \oplus 2_2) \otimes (0 \oplus 4)$. For the octagon edge, we temporarily use a new parametrization (a and b) and later will show how to map it to the previous one (y and z). The state on the octagon edge is set to be $(|0\rangle + a|2_2\rangle)(|0\rangle + b|4\rangle) = |0\rangle + b|4\rangle + a|2_2\rangle + ab|2_1\rangle$.

In this way, we have rewritten the system into two layers of Ising models, see Fig. 12. The Ising model has two Frobenius algebras, and we can use the perfect common module σ on the square edge. We already know that the Ising model reaches the critical point when the octagon edge is tuned to $\langle$  $|+(\sqrt{2}-1)\langle$  $|$. In the current double layer system, we identify 0 as $\mathbf{1}_{\text{Ising}}$, and 2_2 or 4 as ψ_{Ising} in each layer. The first layer represents the competition between 0 and 2_2, while the second layer represents the competition between 0 and 4. The two Ising phase transition lines correspond to the individual critical points for each individual layer. When $a = b = \sqrt{2} - 1$, the two layers are both at the critical point, and the system is self-dual. The system simply stacks two critical Ising models, so the central charge is $c = 1/2 + 1/2 = 1$. In the original parametrization, this point corresponds

to $y = \frac{\sqrt{2}}{3}$ and $z = \frac{1}{3}$, which is exactly the tricritical point at which the two Ising phase transition lines coalesce.

Symmetry Preserving RG of the Strange Correlator

Our construction of the CFT factory is based on the strange correlator formalism. In this approach, a partition function Z is defined as the overlap between a string-net ground state $|\Psi\rangle$ and a tensor network state $\langle\Omega|$ [4](Fig. 13):

$$Z = \langle\Omega|\Psi\rangle. \tag{20}$$

Our choice of $\langle\Omega|$ is a tensor network built from local tensors T^{ABC}_{abc} :

$$\langle\Omega| = \sum_{\{A,B,C\}} \prod_{\mu} T^{ABC}_{abc}(\mu) \langle\{a,b,c\}|. \tag{21}$$

The auxiliary indices $A, B, C \in \{1, 2, \ldots, d_\chi\}$ (blue lines) are summed over all triangles, while the physical indices a, b, c (black lines) are labeled by simple objects and contract with the string-net state $|\Psi\rangle$. Orientation of the fusion rules is indicated by arrows. For convenience, we use an orthonormal basis $\{|\{a,b,c\}\rangle\}$ to denote these open legs. The index μ denotes different triangles.

The string-net ground state admits a tensor-network representation involving tetrahedron symbols [7, 48–50]:

$$|\Psi\rangle = \sum_{\{i,j,k\}} \sqrt{d_a}\, d_i \prod_{\mu} \begin{bmatrix} a & b & c \\ i & j & k \end{bmatrix} (\mu)\, |\{a,b,c\}\rangle. \tag{22}$$

Here the red indices i, j, k are summed over all simple objects in the category. The tetrahedron symbols are related to $6j$-symbols of the UFC by

$$\begin{bmatrix} a & b & c \\ i & j & k \end{bmatrix} = \frac{1}{\sqrt{d_e d_f}} [F^{abi}_{j}]_{ck} = G^{b^* a^* c}_{j i^* k}.$$

Combining $|\Psi\rangle$ with $\langle\Omega|$, the partition function factorizes into local weights:

$$Z = \sum_{\{a,b,c\},\{A,B,C\},\{i,j,k\}} \prod_{\mu} z^{ABC}_{abc,ijk}(\mu), \tag{23}$$

where

$$z^{ABC}_{abc,ijk}(\mu) = \sqrt[4]{d_i^2 d_j d_k^2 d_a d_b d_c}\, T^{ABC}_{abc}(\mu) \begin{bmatrix} a & b & c \\ i & j & k \end{bmatrix} (\mu). \tag{24}$$

We adopt a gauge where tetrahedron symbols are both unitary and tetrahedrally symmetric.[5]. Unitarity implies

$$\sum_{f} d_e d_f \begin{bmatrix} a & b & e \\ c & d & f \end{bmatrix} \begin{bmatrix} a & b & e' \\ c & d & f \end{bmatrix}^* = \delta_{ee'} N^e_{ab} N^d_{ec}, \tag{25}$$

[4]We restrict to real tensors throughout. With complex tensors, conjugation of neighboring tensors would be required, leading to a checkerboard arrangement that ensures reality of the partition function.

[5]Generalization to F-symbols without tetrahedral symmetry is possible, though the RG equations become more involved. We leave this study to future work.

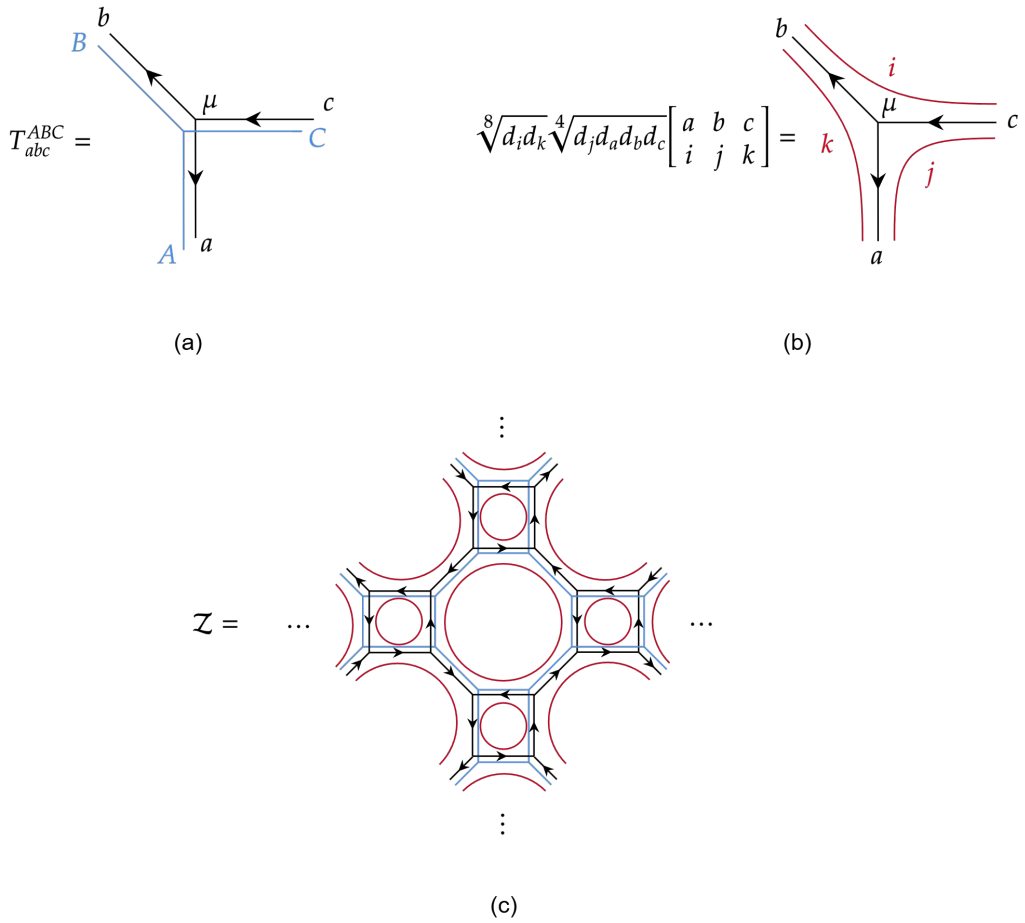


Fig. 13: The strange correlator $\langle\Omega|\Psi\rangle$. (a) Local tensor T^{ABC}_{abc} of state $\langle\Omega|$. (b) Local tensor of state $|\Psi\rangle$, constructed from tetrahedron symbols and quantum dimensions. (c) Their contraction defines the strange correlator. Blue indices are summed within $\langle\Omega|$, red indices within $|\Psi\rangle$, while black physical indices contract between the two.

while tetrahedral symmetry gives identities such as

$$\begin{bmatrix} a & b & e \\ c & d & f \end{bmatrix} = \begin{bmatrix} a^* & e & b \\ c & f & d \end{bmatrix} = \begin{bmatrix} e & b^* & a \\ f & d & c \end{bmatrix} = \begin{bmatrix} a & f & d \\ c^* & e & b \end{bmatrix}. \tag{26}$$

With this symmetry, the pentagon equation takes the form

$$\begin{bmatrix} a & b & e \\ c & d & f \end{bmatrix}\begin{bmatrix} a & b' & e' \\ c' & d & f \end{bmatrix} = \sum_x d_x \begin{bmatrix} a & b & e \\ x & e' & b' \end{bmatrix}\begin{bmatrix} e' & x & e \\ c & d & c' \end{bmatrix}\begin{bmatrix} b' & x & b \\ c & f & c' \end{bmatrix}. \tag{27}$$

The essential virtue of the strange correlator is that deformations of the network $\langle\Omega|$ are precisely the categorical F-moves guaranteed by tetrahedron symbols. Different lattice discretizations are related by these moves, making the construction inherently symmetry-preserving. This feature enables the following RG procedure. In each RG step, four tensors

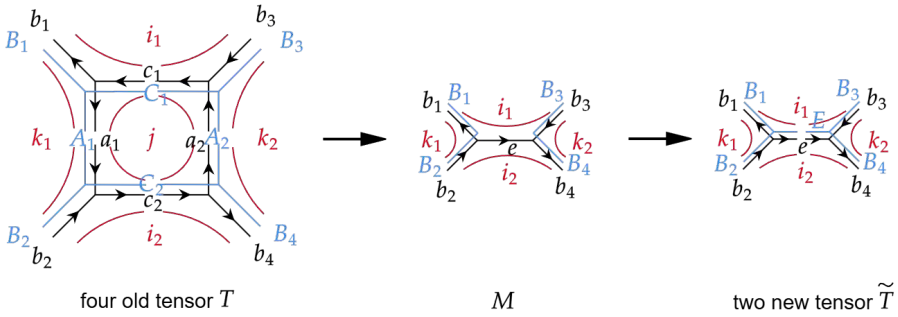


Fig. 14: RG step: four tensors T are combined into an intermediate tensor M, which is then decomposed into two new tensors $\tilde{T}$ via SVD. Red legs indicate tetrahedron-symbol contractions and are not part of T or M.

T are contracted into an intermediate tensor M, which is then factorized by singular value decomposition (SVD) into two renormalized tensors $\tilde{T}$ (Fig. 14).

We begin by rewriting the product of four tetrahedron symbols as follows.

$$\begin{aligned}
&\sum_j d_j \begin{bmatrix} a_1 & b_1 & c_1 \\ i_1 & j & k_1 \end{bmatrix} \begin{bmatrix} a_1 & b_2 & c_2 \\ i_2 & j & k_1 \end{bmatrix} \begin{bmatrix} a_2 & b_3 & c_1 \\ i_1 & j & k_2 \end{bmatrix} \begin{bmatrix} a_2 & b_4 & c_2 \\ i_2 & j & k_2 \end{bmatrix} \\
=&\sum_j d_j \sum_{e_1} d_{e_1} \begin{bmatrix} a_1 & b_2 & c_2 \\ e_1 & c_1 & b_1 \end{bmatrix} \begin{bmatrix} c_1 & e_1 & c_2 \\ i_2 & j & i_1 \end{bmatrix} \begin{bmatrix} b_1 & e_1 & b_2 \\ i_2 & k_1 & i_1 \end{bmatrix} \sum_{e_2} d_{e_2} \begin{bmatrix} a_2 & b_4 & c_2 \\ e_2 & c_1 & b_3 \end{bmatrix} \begin{bmatrix} c_1 & e_2 & c_2 \\ i_2 & j & i_1 \end{bmatrix} \begin{bmatrix} b_3 & e_2 & b_4 \\ i_2 & k_2 & i_1 \end{bmatrix} \\
=&\left(\sum_j d_j \begin{bmatrix} c_1 & e_1 & c_2 \\ i_2 & j & i_1 \end{bmatrix} \begin{bmatrix} c_1 & e_2 & c_2 \\ i_2 & j & i_1 \end{bmatrix} \right) \sum_{e_1,e_2} d_{e_1} d_{e_2} \begin{bmatrix} a_1 & b_2 & c_2 \\ e_1 & c_1 & b_1 \end{bmatrix} \begin{bmatrix} b_1 & e_1 & b_2 \\ i_2 & k_1 & i_1 \end{bmatrix} \begin{bmatrix} a_2 & b_4 & c_2 \\ e_2 & c_1 & b_3 \end{bmatrix} \begin{bmatrix} b_3 & e_2 & b_4 \\ i_2 & k_2 & i_1 \end{bmatrix} \\
=&\sum_e \sqrt{d_e} \begin{bmatrix} b_1 & e & b_2 \\ i_2 & k_1 & i_1 \end{bmatrix} \begin{bmatrix} b_3 & e & b_4 \\ i_2 & k_2 & i_1 \end{bmatrix} \left(\sqrt{d_e} \begin{bmatrix} a_1 & b_2 & c_2 \\ e & c_1 & b_1 \end{bmatrix} \begin{bmatrix} a_2 & b_4 & c_2 \\ e & c_1 & b_3 \end{bmatrix} \right).
\end{aligned} \tag{28}$$

Here, the second row is due to (27), and the fourth line is due to (25) and a sum over $\delta_{e_1 e_2}$. We combine the factors in brackets with tensor T to get an intermediate tensor M:

$$M^{B_1B_2B_3B_4}_{b_1b_2b_3b_4e} = \sum_{a_1,a_2,c_1,c_2}^{A_1,A_2,C_1,C_2} \sqrt{d_{a_1} d_{a_2} d_{c_1} d_{c_2} d_e} \begin{bmatrix} a_1 & b_2 & c_2 \\ e & c_1 & b_1 \end{bmatrix} \begin{bmatrix} a_2 & b_4 & c_2 \\ e & c_1 & b_3 \end{bmatrix} T^{A_1B_1C_1}_{a_1b_1c_1} T^{A_1B_2C_2}_{a_1b_2c_2} T^{A_2B_3C_1}_{a_2b_3c_1} T^{A_2B_4C_2}_{a_2b_4c_2}. \tag{29}$$

A new tensor $\tilde{T}$ is then obtained by applying a singular value decomposition (SVD) to the tensor M,

$$M^{B_1B_2B_3B_4}_{b_1b_2b_3b_4e} = \sum_E \tilde{T}^{B_1EB_2}_{b_1eb_2} \tilde{T}^{B_3EB_4}_{b_3eb_4}. \tag{30}$$

This procedure is practically implemented via gradient-descents based loop-TNR [51] to search for an optimal approximation within a given bond dimension of the new index E.

In total, each RG step is expressed as

$$\sum_e^E \sqrt{d_e} \begin{bmatrix} b_1 & e & b_2 \\ i_2 & k_1 & i_1 \end{bmatrix} \begin{bmatrix} b_3 & e & b_4 \\ i_2 & k_2 & i_1 \end{bmatrix} \tilde{T}^{B_1EB_2}_{b_1eb_2} \tilde{T}^{B_3EB_4}_{b_3eb_4} = \sum_{a_1,a_2,c_1,c_2,j}^{A_1,A_2,C_1,C_2} \sqrt{d_{a_1} d_{a_2} d_{c_1} d_{c_2}} d_j$$

$$\begin{bmatrix} a_1 & b_1 & c_1 \\ i_1 & j & k_1 \end{bmatrix} \begin{bmatrix} a_1 & b_2 & c_2 \\ i_2 & j & k_1 \end{bmatrix} \begin{bmatrix} a_2 & b_3 & c_1 \\ i_1 & j & k_2 \end{bmatrix} \begin{bmatrix} a_2 & b_4 & c_2 \\ i_2 & j & k_2 \end{bmatrix} T^{A_1B_1C_1}_{a_1b_1c_1} T^{A_1B_2C_2}_{a_1b_2c_2} T^{A_2B_3C_1}_{a_2b_3c_1} T^{A_2B_4C_2}_{a_2b_4c_2}. \tag{31}$$

The original form of the strange correlator is preserved after a complete RG step, with each tensor T flowing to $\tilde{T}$. The categorical symmetry, as imposed by the 3D bulk that is carried throughout the RG process, is thus preserved in the RG procedure. The orientated fusions at the new vertices are $b_1 \otimes e \to b_2$ and $b_3 \otimes e \to b_4$. One can alternatively obtain $b_2 \otimes e' \to b_1$ and $b_4 \otimes e' \to b_3$ by applying a different set of the pentagon equation in 28.

In our setup, a unit cell typically consists of two local T tensors. The initial tensor for the RG flow can be considered as the tensor M in (29) and (30). Consequently, an initial decomposition step of (30) is performed. Explicitly, for unit cells corresponding to (6), where each $\langle$  | is weighted by parameter r_i, the initial tensor M is

$$M_{b_1b_2b_3b_4e} = \sum_i r_i [\rho_{M_{\mathcal{A}_i}}]^e_{b_1b_2} ([\rho_{M_{\mathcal{A}_i}}]^e_{b_3b_4})^*. \tag{32}$$

Here, auxiliary legs B_i are omitted in M. For general initial tensors, B_i and possibly also E account for multiplicities if a simple object b_i or e appear multiple times in $M_{\mathcal{A}}$ or $\mathcal{A}$. In present cases, the multiplicity is no more than 1, so the initial tensor has trivial auxiliary legs. During the RG procedure, the auxiliary legs' effective bond dimensions can increase, reflecting the growing entanglement among the local tensors.

Computing the Phase Diagram

If the initial tensor corresponds to a single Frobenius algebra, the RG flow converges in one step to its multiplication $f^{\mathcal{A}}$, which is a fixed point tensor. General gapped-state tensors flow to one of these fixed points, providing an order parameter that distinguishes phases. Phase diagrams obtained this way show excellent accuracy even at minimal bond dimension $d_\chi = 1$ (Fig. 15), illustrating the efficiency of the categorical symmetric RG.

Central charges are extracted from transfer matrices built from coarse-grained tensors, following [52]. In practice, bond dimensions $d_\chi = 4$–20 are used, depending on the model. Central charges typically stabilize after ~ 6 RG steps, with each step taking 5–15 seconds on a Tesla V100 GPU.

Central charges can also be represented as phase diagrams whenever the phase transitions are governed by CFTs. For conventional first-order phase transitions, the central charge is expected to vanish. In practice, however, we also encounter weak first-order transitions that are very close to second-order ones [35, 36]. In such cases, the computed central charge typically remains finite after a moderate number of RG steps (about 10–20, depending on the model), which explains the appearance of nonzero residuals at some first-order phase boundaries.

A further characteristic is that certain first-order transitions exhibit oscillatory behavior in the extracted central charge—both along the RG flow and across the phase diagram. In the 5-state Potts model, we read off an oscillatory central charge around an average value of $c \approx 1.1$ at the first order phase transition point, consistent with the real part of the associated complex CFT. The latter has been identified as $c \approx 1.138 \pm 0.021i$ [53, 54].

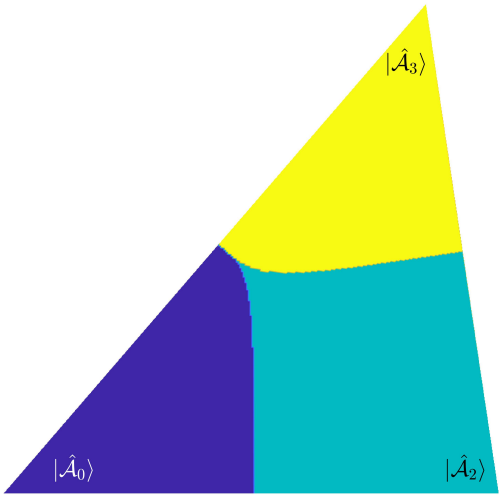


Fig. 15: Ternary phase diagram for the interpolation of algebras $\mathcal{A}_{0,2,3}$ under module 2 of the A_5 category. Different colors correspond to different converged fixed-point tensors, computed with $d_\chi = 1$. This illustrates the role of the fixed-point tensor as an order parameter, highlighting the precision of our RG scheme even at a small bond dimension.

In the phase diagram, the oscillations manifest as two closely separated lines on the critical boundary, as illustrated in Fig.6 and Fig.8. We conjecture that such oscillatory central charges signal the proximity of complex CFTs.

While our present algorithm already achieves high resolution for the phase diagrams, there remains considerable room for improving the extraction of critical data. We leave more elaborate developments to future work.

Comments on More Complicated Boundary Conditions and Enlarging the Unit Cell

A salient question is how to generalise our construction to other lattices. Our choice of square lattice is to ensure that there is an equal number of plaquettes and vertices, making the equal weight summation of competing condensates a natural location of criticality because we need not to distinguish fluxons and chargeons, which supposedly reside on on vertices and in plaquettes respectively. For more generic lattices, we suspect that the equal mixture of competing condensates may not always generate a critical state globally. The correct relative weights may depend on the ratio of plaquettes and vertices in the given lattice. This certainly deserves future exploration.

Another important question is how to explore the effect of enlarging the unit cell.

In this paper, we have chosen a minimal unit cell, and explored the phase space of theories by varying couplings within the unit cell, which is obviously only a small corner of possible theories that realise the given symmetries. Hence, two paramount questions are

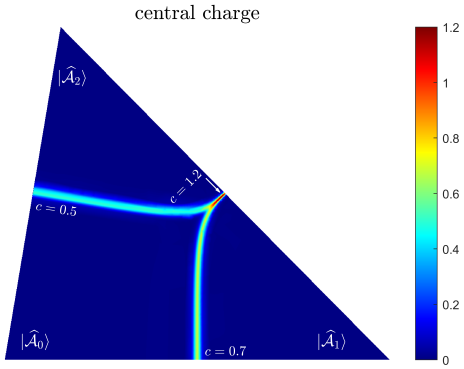


Fig. 16: The ternary phase diagram of interpolating the Frobenius algebras $\mathcal{A}_0 = 0, \mathcal{A}_1 = 0 \oplus 2, \mathcal{A}_2 = 0 \oplus 3$ with module $1 \oplus 2$ in category A_4. They are all subalgebras of $\mathcal{A}_3 = 0 \oplus 1 \oplus 2 \oplus 3$. Each phase is marked by one of the three nomalised states $\mathcal{A}_i$. The three phases are seperated by the critical lines with central charge $c > 0$. This is another illustration of the double-layer structure, see main text for details.

1) what the possible systems that can be realised within this restricted phase space are, and 2) how to systematically enlarge the space of theories that one explores.

To the first question, we observe that when the phase subspace gets smaller, the central charge of the resultant critical point also appears to be smaller. For example, the A-series were realised by picking a module that essentially reduce the phase space in the unit cell to 2-dimensions. In that case, the central charge of the resultant critical point seems to be smaller than that with the same choice of unit cell but a large phase space. The number of degrees of freedom involved in the unit cell seems to be related to the central charge of any realised critical point. We suspect that the "canonical" CFT for a given symTO proposed in [22] can always be realised from models constructed in the unit cell.

This observation can be qualitatively explained by the generalised KW duality. As one increases the dimension of the subspace, the degrees of freedom often fall into decoupled multi-layer system, a direct generalisation of the double-layer structure described in the text. The CFT at the critical point of the multi-layer system is a tensor product of the CFTs of each critical layer; hemce, the central charge is larger. Apart from the exmaples above, a $c = 1.2$ CFT is observed in category A_4 as plotted in Fig. 16. This CFT is realised in a subspace of 4 dimensions. From the generalised KW duality, this system can be decomposed into a double layer, each bearing a 2-dimensional subspace. The two layers contribute a $c = 0.5$ CFT and a $c = 0.7$ CFT when both layers are tuned to its respective critical point. The observed $c = 1.2$ CFT should simply be the stacking of the two single-layer CFTs.

As the chosen unit cell's size increases, one expects that the strange correlator should be able to describe more complicated CFTs carrying the symmetries with larger central charges. We considered a larger unit cell as shown in Fig. 17.

We observe that generalised KW duality can effectively search for critical points here.

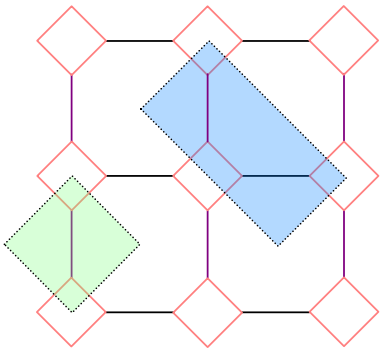


Fig. 17: Example of a larger unit cell. The blue region is the unit cell of the anisotropic state $\langle\Omega|$, of which the horizontal and vertical edges are in general different. If $\langle\Omega|$ is isotropic, then the unit cell is the green region, which is discussed extensively in the text above.

The KW duality exchanges squares with octagons and swaps horizontal edges with vertical ones. On enlarging the unit cell to accomodate the anisotropic $\langle\Omega|$, the n-dimensional phase space is promoted to a $2n$-dimensional phase space. In general, the critical self-dual manifold in the n-dimensional phase diagram is promoted to a critical self-dual manifold with higher dimensions in the $2n$-dimensional phase diagram. The extra dimensions of the critical manifold are often irrelevant to the CFT. We have checked this in the case of Ising, Fibonacci, and A_k categories and the results will be presented elsewhere.

Larger unit cells can be converted to an entangled $\langle\Omega|$ state and computed by the same numerical RG process. We have not yet looked into a more general ansatz to systematically produce critical models for $\langle\Omega|$ that carries entanglement. This and other important questions will be discussed elsewhere.

Acknowledgments

The authors thank Rui-Zhen Huang, Yunfeng Jiang, Zhengwei Liu, Shuang Ming, Sébastien Palcoux, Yilong Wang, Jinsong Wu, Zhihao Zhang for inspiring and helpful discussions. LYH is supported by NSFC (Grant No. 11922502, 11875111). CS is supported by the postdoctoral fund of Beijing Institute of Mathematical Sciences and Applications. Part of this work was done during the KITP Program "generalised Symmetries in Quantum Field Theory: High Energy Physics, Condensed Matter, and Quantum Gravity", and supported in part by grant NSF PHY-2309135 to the Kavli Institute for Theoretical Physics (KITP). YW is supported by NSFC Grant No. KRH1512711, the Shanghai Municipal Science and Technology Major Project (Grant No. 2019SHZDZX01), Science and Technology Commission of Shanghai Municipality (Grant No. 24LZ1400100), and the Innovation Program for Quantum Science and Technology (No. 2024ZD0300101). YW is grateful for the hospitality of the Perimeter Institute during his visit, where the main part of this work is done. This research was supported in part by the Perimeter Institute for Theoretical Physics. Research at Perimeter Institute is supported by the Government of Canada through the

Department of Innovation, Science and Economic Development and by the Province of Ontario through the Ministry of Research, Innovation and Science. LYH acknowledges Lin Chen, Yikun Jiang, Bingxin Lao for collaboration and discussions on related problems.

Author contributions

L.-Y.H. conceived and supervised the project. Y.W. co-supervised the project. L.-Y.H., Y.W., and Y.Z. initiated the first working examples combining the strange-correlator and competing-anyon-condensation approaches. Y.Z. applied anyon-condensation formalism in the string-net model. C.S. worked out the classification of algebras and modules, formulated the generalised Kramers–Wannier duality, and performed initial numerical verification of key critical points. Y.Z., K.J. and C.S. obtained the algebra and module data used in the numerics. K.J. developed and implemented the symmetry-preserving tensor network algorithms, generated all numerical phase diagrams and derived the equation for predicting general phase boundaries. All authors discussed the results extensively and contributed to the drafting and revising of the manuscript.

Data availability

The numerical datasets generated and analysed during this study are available in the figshare repository at doi.org/10.6084/m9.figshare.29974867.v1. The custom code used in this study is available from the authors upon request.

References

[1] D. Bernard and G. Felder, "Quantum group symmetries in 2-D lattice quantum field theory," *Nucl. Phys. B* **365** (1991) 98–120.

[2] M. A. Rajabpour and J. Cardy, "Discretely Holomorphic Parafermions in Lattice Z_N Models," *J. Phys. A* **40** (2008) 14703–14713, arXiv:0708.3772 [math-ph].

[3] Y. Ikhlef and R. Weston, "Discrete Holomorphicity in the Chiral Potts Model," *J. Phys. A* **48** no. 29, (2015) 294001, arXiv:1502.04944 [math-ph].

[4] P. Fendley, "Integrability and braided tensor categories," *J. Statist. Phys.* **182** (2021) 43, arXiv:2008.02292 [math-ph].

[5] A. Feiguin, S. Trebst, A. W. W. Ludwig, M. Troyer, A. Kitaev, Z. Wang, and M. H. Freedman, "Interacting anyons in topological quantum liquids: The golden chain," *Phys. Rev. Lett.* **98** (2007) 160409, arXiv:cond-mat/0612341.

[6] D. Aasen, R. S. K. Mong, and P. Fendley, "Topological Defects on the Lattice I: The Ising model," *J. Phys. A* **49** no. 35, (2016) 354001, arXiv:1601.07185 [cond-mat.stat-mech].

[7] D. Aasen, P. Fendley, and R. S. K. Mong, "Topological Defects on the Lattice: Dualities and Degeneracies," arXiv:2008.08598 [cond-mat.stat-mech].

[8] R. Vanhove, M. Bal, D. J. Williamson, N. Bultinck, J. Haegeman, and F. Verstraete, "Mapping topological to conformal field theories through strange correlators," *Phys. Rev. Lett.* **121** no. 17, (2018) 177203, arXiv:1801.05959 [quant-ph].

[9] Y.-Z. You, Z. Bi, A. Rasmussen, K. Slagle, and C. Xu, "Wave function and strange correlator of short-range entangled states," *Physical Review Letters* **112** no. 24, (June, 2014) . http://dx.doi.org/10.1103/PhysRevLett.112.247202.

[10] S.-Q. Ning, B.-B. Mao, and C. Wang, "Building 1D lattice models with G-graded fusion category," *SciPost Phys.* **17** (2024) 125. https://scipost.org/10.21468/SciPostPhys.17.5.125.

[11] W.-T. Xu, Q. Zhang, and G.-M. Zhang, "Tensor network approach to phase transitions of a non-abelian topological phase," *Physical Review Letters* **124** no. 13, (2020) 130603.

[12] J.-Y. Zhang, M.-Y. Li, and P. Ye, "Higher-Order Cellular Automata Generated Symmetry-Protected Topological Phases and Detection Through Multi Point Strange Correlators," *PRX Quantum* **5** no. 3, (2024) 030342, arXiv:2401.00505 [cond-mat.str-el].

[13] D.-C. Lu, F. Xu, and Y.-Z. You, "Strange correlator and string order parameter for non-invertible symmetry protected topological phases in 1+1d," arXiv:2505.00673 [cond-mat.str-el].

[14] W. Ji and X.-G. Wen, "Categorical symmetry and noninvertible anomaly in symmetry-breaking and topological phase transitions," *Phys. Rev. Res.* **2** no. 3, (2020) 033417, arXiv:1912.13492 [cond-mat.str-el].

[15] L. Kong, T. Lan, X.-G. Wen, Z.-H. Zhang, and H. Zheng, "Algebraic higher symmetry and categorical symmetry – a holographic and entanglement view of symmetry," *Phys. Rev. Res.* **2** no. 4, (2020) 043086, arXiv:2005.14178 [cond-mat.str-el].

[16] L. Kong, T. Lan, X.-G. Wen, Z.-H. Zhang, and H. Zheng, "Classification of topological

phases with finite internal symmetries in all dimensions," *JHEP* **09** (2020) 093, arXiv:2003.08898 [math-ph].

[17] D. Gaiotto and J. Kulp, "Orbifold groupoids," *JHEP* **02** (2021) 132, arXiv:2008.05960 [hep-th].

[18] D. S. Freed, G. W. Moore, and C. Teleman, "Topological symmetry in quantum field theory," arXiv:2209.07471 [hep-th].

[19] F. Apruzzi, F. Bonetti, I. n. García Etxebarria, S. S. Hosseini, and S. Schafer-Nameki, "Symmetry TFTs from String Theory," *Commun. Math. Phys.* **402** no. 1, (2023) 895–949, arXiv:2112.02092 [hep-th].

[20] A. Chatterjee and X.-G. Wen, "Symmetry as a shadow of topological order and a derivation of topological holographic principle," *Phys. Rev. B* **107** no. 15, (2023) 155136, arXiv:2203.03596 [cond-mat.str-el].

[21] D. S. Freed and C. Teleman, "Topological dualities in the Ising model," *Geom. Topol.* **26** (2022) 1907–1984, arXiv:1806.00008 [math.AT].

[22] L. Kong and H. Zheng, "A mathematical theory of gapless edges of 2d topological orders. Part I," *JHEP* **02** (2020) 150, arXiv:1905.04924 [cond-mat.str-el].

[23] L. Bhardwaj and Y. Tachikawa, "On finite symmetries and their gauging in two dimensions," *JHEP* **03** (2018) 189, arXiv:1704.02330 [hep-th].

[24] R. Vanhove, L. Lootens, M. Van Damme, R. Wolf, T. J. Osborne, J. Haegeman, and F. Verstraete, "Critical Lattice Model for a Haagerup Conformal Field Theory," *Phys. Rev. Lett.* **128** no. 23, (2022) 231602, arXiv:2110.03532 [cond-mat.stat-mech].

[25] T.-C. Huang, Y.-H. Lin, K. Ohmori, Y. Tachikawa, and M. Tezuka, "Numerical Evidence for a Haagerup Conformal Field Theory," *Phys. Rev. Lett.* **128** no. 23, (2022) 231603, arXiv:2110.03008 [cond-mat.stat-mech].

[26] M. A. Levin and X.-G. Wen, "String net condensation: A Physical mechanism for topological phases," *Phys. Rev. B* **71** (2005) 045110, arXiv:cond-mat/0404617.

[27] M. Levin and Z.-C. Gu, "Braiding statistics approach to symmetry-protected topological phases," *Physical Review B* **86** no. 11, (Sept., 2012) . http://dx.doi.org/10.1103/PhysRevB.86.115109.

[28] M. Levin, "Constraints on order and disorder parameters in quantum spin chains," *Commun. Math. Phys.* **378** no. 2, (2020) 1081–1106, arXiv:1903.09028 [cond-mat.str-el].

[29] M. Levin, "Protected Edge Modes without Symmetry," *Physical Review X* **3** no. 2, (Apr., 2013) 021009, arXiv:1301.7355 [cond-mat.str-el].

[30] Y. Hu, N. Geer, and Y.-S. Wu, "Full dyon excitation spectrum in extended Levin-Wen models," *Phys. Rev. B* **97** no. 19, (2018) 195154, arXiv:1502.03433 [cond-mat.str-el].

[31] Y. Zhao, H. Wang, Y. Hu, and Y. Wan, "Symmetry fractionalized (irrationalized) fusion rules and two domain-wall verlinde formulae," *Journal of High Energy Physics* **2024** no. 4, (2024) 1–26.

[32] Y. Zhao and Y. Wan, "Nonabelian anyon condensation in 2+1d topological orders: A string-net model realization," *JHEP* **05** (2025) 156, arXiv:2409.05852 [cond-mat.str-el].

[33] L. Chen, K. Ji, H. Zhang, C. Shen, R. Wang, X. Zeng, and L.-Y. Hung, "CFTD from

TQFTD+1 via Holographic Tensor Network, and Precision Discretization of CFT2 ," *Phys. Rev. X* **14** no. 4, (2024) 041033, arXiv:2210.12127 [hep-th].

[34] N. Bao, L.-Y. Hung, Y. Jiang, and Z. Liu, "QG from SymQRG: AdS_3/CFT_2 Correspondence as Topological Symmetry-Preserving Quantum RG Flow," arXiv:2412.12045 [hep-th].

[35] D. B. Kaplan, J. W. Lee, D. T. Son, and M. A. Stephanov, "Conformality lost," *Int. J. Mod. Phys. A* **25** (2010) 422–432.

[36] A. F. Faedo, C. Hoyos, D. Mateos, and J. G. Subils, "Holographic Complex Conformal Field Theories," *Phys. Rev. Lett.* **124** no. 16, (2020) 161601, arXiv:1909.04008 [hep-th].

[37] P. Grossman and N. Snyder, "Quantum subgroups of the haagerup fusion categories," *Communications in Mathematical Physics* **311** (2012) 617–643.

[38] M. Asaeda and U. Haagerup, "Exotic subfactors of finite depth with jones indices $(5+\sqrt{13})/2$ and $(5+\sqrt{17})/2$," *Communications in mathematical physics* **202** no. 1, (1999) 1–63.

[39] L. E. Bottini and S. Schafer-Nameki, "A Gapless Phase with Haagerup Symmetry," arXiv:2410.19040 [hep-th].

[40] M. Kohmoto, M. Den Nijs, and L. P. Kadanoff, "Hamiltonian studies of the d = 2 Ashkin-Teller model," *Physical Review B* **24** no. 9, (Nov., 1981) 5229–5241.

[41] A. M. Mariz, C. Tsallis, and P. Fulco, "Z(4) model: Criticality and break-collapse method," *Physical Review B* **32** no. 9, (Nov., 1985) 6055–6057.

[42] C. Shen, "Exploring the phase diagram of $SU(2)_4$ strange correlator," *arXiv preprint arXiv:2502.14556* (2025) .

[43] Y. Zhao and Y. Wan, "Landau-ginzburg paradigm of topological phases," *arXiv preprint arXiv:2506.05319* (2025) .

[44] L. Bhardwaj, D. Pajer, S. Schafer-Nameki, and A. Warman, "Hasse Diagrams for Gapless SPT and SSB Phases with Non-Invertible Symmetries," arXiv:2403.00905 [cond-mat.str-el].

[45] F. C. Alcaraz and R. Koberle, "The Phases of Two-dimensional Spin and Four-dimensional Gauge Systems With $Z(N)$ Symmetry," *J. Phys. A* **14** (1981) 1169.

[46] H. Wang, Y. Li, Y. Hu, and Y. Wan, "Electric-magnetic duality in the quantum double models of topological orders with gapped boundaries," *Journal of High Energy Physics* **2020** no. 2, (2020) 1–43.

[47] Y. Hu and Y. Wan, "Electric-magnetic duality in twisted quantum double model of topological orders," *Journal of High Energy Physics* **2020** no. 11, (2020) 1–39.

[48] O. Buerschaper, M. Aguado, and G. Vidal, "Explicit tensor network representation for the ground states of string-net models," *Phys. Rev. B* **79** (Feb, 2009) 085119. https://link.aps.org/doi/10.1103/PhysRevB.79.085119.

[49] Z.-C. Gu, M. Levin, B. Swingle, and X.-G. Wen, "Tensor-product representations for string-net condensed states," *Phys. Rev. B* **79** (Feb, 2009) 085118. https://link.aps.org/doi/10.1103/PhysRevB.79.085118.

[50] R. Vanhove, L. Lootens, H.-H. Tu, and F. Verstraete, "Topological aspects of the critical three-state Potts model," *J. Phys. A* **55** no. 23, (2022) 235002, arXiv:2107.11177 [math-ph].

[51] S. Yang, Z.-C. Gu, and X.-G. Wen, "Loop optimization for tensor network renormalization," *Physical Review Letters* **118** no. 11, (Mar., 2017) . http://dx.doi.org/10.1103/PhysRevLett.118.110504.

[52] Z.-C. Gu and X.-G. Wen, "Tensor-entanglement-filtering renormalization approach and symmetry-protected topological order," *Physical Review B—Condensed Matter and Materials Physics* **80** no. 15, (2009) 155131.

[53] V. Gorbenko, S. Rychkov, and B. Zan, "Walking, Weak first-order transitions, and Complex CFTs," *JHEP* **10** (2018) 108, arXiv:1807.11512 [hep-th].

[54] V. Gorbenko, S. Rychkov, and B. Zan, "Walking, Weak first-order transitions, and Complex CFTs II. Two-dimensional Potts model at $Q > 4$," *SciPost Phys.* **5** no. 5, (2018) 050, arXiv:1808.04380 [hep-th].

Supplementary Files

This is a list of supplementary files associated with this preprint. Click to download.

- NewCFTsupplementary.pdf